RSC Advances

REVIEW

View Article Online
View Journal | View Issue

Cite this: *RSC Adv.*, 2016, **6**, 64993

Graphene oxide: strategies for synthesis, reduction and frontier applications

Rajesh Kumar Singh,[a] Rajesh Kumar*[b] and Dinesh Pratap Singh*[c]

Till now, several innovative methods have been developed for the synthesis of graphene materials including mechanical exfoliation, epitaxial growth by chemical vapor deposition, chemical reduction of graphite oxide, liquid-phase exfoliation, arc discharge of graphite, *in situ* electron beam irradiation, epitaxial growth on SiC, thermal fusion, laser reduction of polymers sheets and unzipping of carbon nanotubes *etc.* Generally large scale graphene nanosheets are reliably synthesized utilizing other forms of graphene-based novel materials, including graphene oxide (GO), exfoliated graphite oxide (by thermal and microwave), and reduced graphene oxide. The degree of GO reduction and number of graphene layers are minimized mainly by applying two approaches *via* chemical or thermal treatments. The promising and excellent properties together with the ease of processability and chemical functionalization makes graphene based materials especially GO, ideal candidates for incorporation into a variety of advanced functional materials. Chemical functionalization of graphene can be easily achieved, by the introduction of various functional groups. These functional groups help to control and manipulate the graphene surfaces and help to tune the properties of the resulting hybrid materials. Importantly, graphene and its derivatives GO, have been explored in a wide range of applications, such as energy generation/storage, optical devices, electronic and photonic devices, drug delivery, clean energy, and chemical/bio sensors. In this review article, we have incorporated a general introduction of GO, its synthesis, reduction and some selected frontier applications.

Received 23rd March 2016
Accepted 27th June 2016

DOI: 10.1039/c6ra07626b

www.rsc.org/advances

[a]*School of Physical & Material Sciences, Central University of Himachal Pradesh (CUHP), Kangra, Dharamshala, HP-176215, India*

[b]*Center for Semiconductor Components and Nanotechnology (CCS Nano), University of Campinas (UNICAMP), 13083-870 Campinas, Sao Paulo, Brazil. E-mail: rajeshbhu1@gmail.com*

[c]*Departamento de Física, Universidad de Santiago de Chile, Avenida Ecuador 3493, Estación Central, Santiago 9170124, Chile. E-mail: dineshpsingh@gmail.com*

Rajesh Kumar Singh is an Asst. Professor in the School of Physical and Material Sciences, Central University of Himachal Pradesh, India. He obtained his Ph.D. (2011) degree in Physics from Institute of Sciences, Banaras Hindu University (B.H.U) Varanasi, India. He then spent 4 years (2011–2015) at the Indian Institute of Technology (B.H.U.) Varanasi as a post-doctoral fellow. His current research interests include hydrogen storage, solid oxide fuel cells, synthesis of carbon nanostructures-metal/metal oxide self-assembly and their applications in different areas. He has published one international book chapter, two review and several peer-reviewed international papers.

Rajesh Kumar is a Postdoctoral Fellow in the Center for Semiconductor Components and Nanotechnology, University of Campinas (UNICAMP), Sao Paulo, Brazil. He received his B.S and M.S. (Physics) degree from Allahabad University, India. He earned his Ph.D. (Physics) (2011) degree from Department of Physics, Banaras Hindu University (B.H.U), India. He has worked in KAIST, Daejeon (Postdoctoral Researcher) and Yonsei University (Research Professor), Seoul, South Korea. His main research interests are the synthesis, characterization, modifications, assemblies and applications of the graphitic carbon nano-materials as graphene and CNTs. He has published two international book chapters, two review articles and several research articles in peer-reviewed international journals.

1. Introduction

Graphene is an exciting material of the 21st century, which has a one-atom-thick 1D planar sheet of sp^2-bonded carbon atoms in a honeycomb crystal lattice with exceptionally high crystal quality and electronic properties which has emerged as a rapidly rising star in the field of material science.[1–5] It is also known as the mother element of carbon allotropes, including graphite, carbon nanotubes, and fullerenes.[3,6] Its peculiar properties such as high intrinsic mobility,[7,8] thermal conductivity,[9] high theoretical specific surface area,[10] high Young's modulus,[11] high optical transmittance[12] and good electrical conductivity[13] merit attention for various novel potential applications. These properties were experimentally studied and verified in last several decades[14–19] and various top-up and bottom-up synthesis approach have been developed for high quality graphene using micromechanically exfoliation of graphite layers,[20] graphene grown on 6H–SiC,[21] large area graphene grown on copper substrates[22] *etc.*

Nowadays, graphene can be produced by micro-mechanical exfoliation of highly ordered pyrolytic graphite,[20] epitaxial growth,[17,23,24] and chemical vapor deposition (CVD).[25,26] These three methods can produce graphene with a relatively perfect structure and excellent properties. However in comparison, graphene produced by reduction of graphene oxide (GO) has some important characteristics as it is produced using graphite material by cost-effective chemical methods in large scale. It is also highly hydrophilic and forms stable aqueous colloids to facilitate the assembly of macroscopic structures by simple and cheap solution processes. As a result, GO and reduced GO (rGO) are still hot topics in the research area and development of graphene, especially in regard to mass applications.

Synthesis of graphite oxide by oxidation of graphite through various chemical routes is the fundamental need for graphene-based materials. GO and graphene are highly promising for various applications due to their unusual thermal, electrical and optical properties. GO produced from graphite using various chemical oxidation routes,[27–30] has attracted considerable attention as a potential material for use in various industrial applications such as photovoltaic cells, capacitors, sensors, and transparent electrodes.[31–35] One particular branch of graphene research deals with GO and graphene synthesized from graphite oxide. Graphite oxide is generally obtained by oxidation of natural graphite powder with various oxidants in acidic media.

The presence of several groups like epoxy, hydroxyl, carboxyl and carbonyl on GO are well recognised and accepted as major functionalities attached to it. Several structural models of graphite oxide comprising these groups have been reported so far in the literature.[36–39] GO can be considered as a precursor for graphene synthesis by either chemical, thermal or microwave reduction processes. GO consists of a 1D single-layer of graphite oxide and is usually produced by the chemical treatment of graphite through oxidation.[36,40] The GO mainly consists of individual sheets of graphene with attachments of oxygen functional groups on both the basal planes and edges.[41] It has different structural models and contains various oxygen functional groups on its surfaces. The oxygen functional groups have been identified as hydroxyl and epoxy groups present on the basal plane, carboxy, carbonyl, and phenol groups at the edge of GO sheets.[42–44] For the synthesis of GO, we first need to synthesize graphite oxide by different chemical process route.

Dr. Dinesh Pratap Singh received M.Sc. (2000) and Ph.D. (2007) degree in Physics from the Banaras Hindu University (B.H.U), Varanasi India. After post-doctoral studies from Southern Illinois University Carbondale, Illinois, USA, he became an assistant professor of Physics at University of Santiago in Chile (2010). His current research interests include, graphene based solar cells, synthesis of nanomaterials, high temperature nanotribology and biomedical applications of nanomaterials. He has published several refereed journal articles, review articles and book chapters.

2. Synthesis of graphene/graphite oxide: oxidation of bulk graphite powder

From last several years, both theoretically and experimentally, considerable effort has been directed toward understanding the structure of graphite oxide. The GO is currently the most common precursor used for the synthesis of graphene materials. The focused study of the GO structure is derived from the structural analysis of graphite oxide itself. Its can be prepared by the intercalation and oxidation of graphite powder. For synthesis of GO in bulk amount, we first need to synthesize graphite oxide applying any of the methods discussed below. The history of GO is very interesting especially when we deal with its synthesis. The first report on the synthesis of GO by the intercalation of graphite sheets was given by a Schafhacutl in 1840. Schafhacutl for the very first time attempted to exfoliate graphite, when he tried to purify the impure graphite "kish" from iron smelters.[45–47]

The well known methods used for the synthesis of graphite oxide are Brodie method,[27] Staudenmaier method,[29] Hofmann method[30,48] and Hummers method[28] and also their modified and improved forms. In these methods, initially graphite powder is chemically reacted with acids (HCl, H_2SO_4 and HNO_3 *etc.*) followed by the intercalation of alkali metals (alkali metal compounds $KClO_3$, $KMnO_4$, $NaNO_3$ *etc.*) into the graphitic layers which further helps in the breaking of graphitic layers into small pieces.

2.1. Brodie's oxidation method

The oxidation of graphite in the presence of potassium chlorate ($KClO_3$) and fuming nitric acid was developed by B.C. Brodie in

1859. He was the pioneering one who treated graphitic powder with $KClO_3$ in concentrated fuming HNO_3 (ref. 27) and got a new compound which later on was determined to contain carbon, oxygen and hydrogen resulting in an increase in the overall mass of the flake graphite. He isolated the crystals of the material, but the interfacial angles of the crystal lattice were unable to be measured *via* reflective goniometry. Successive oxidative treatments resulted in a further increase in the oxygen content, reaching a limit after several reactions. The C : H : O percentage composition was determined to be 61.04 : 1.85 : 37.11. According to his elemental analysis, the molecular formula for the final product was $C_{11}H_4O_5$. He found that the as synthesized material are dispersible in basic or pure water, but not in acidic media, which prompted him to term the material as graphic acid. After heating (220 °C), the C : H : O composition of this material changed to 80.13 : 0.58 : 19.29, with a loss of carbonic acid and carbonic oxide. This method has several flaws including long reaction time as well as release of toxic gases during reaction. Although some research groups used this method for the production of graphite oxide and cited in their published literature.[36,49–54]

2.2. Staudenmaier method: fuming HNO_3, concentrated H_2SO_4 acid and $KClO_3$

One of the improvements on Brodie's work happened in 1898 by L. Staudenmaier using excess of the oxidizing agent and concentrated sulfuric acid as extra additive.[29] He improves the Brodie's $KClO_3$-fuming HNO_3 preparation by (i) adding multiple aliquots of potassium chlorate solution into the reaction mixture over the course of reaction and adding concentrated sulfuric acid (H_2SO_4) to increase the acidity of the mixture. These changes led to a highly oxidized graphite oxide in a single reaction vessel, thus simplified the GO synthesis process. This slight change in the synthesis procedure resulted in an overall extent of oxidation similar to Brodie's multiple oxidation approach (C : O ~ 2 : 1). However, this Staudenmaier's preparation method was time consuming and hazardous: the addition of potassium chlorate typically lasted over a week, and the chlorine dioxide evolved needed to be removed by an inert gas, while explosion was a constant hazard. Therefore, the further modification or development of the new process for oxidation was still under investigation. This method and its modified form has also been used by several other groups for the synthesis of graphite oxide.[55–60]

2.3. Hofmann method: concentrated HNO_3 acid, concentrated H_2SO_4 acid and $KClO_3$

In 1937, Hofmann *et al.*[30,48] used concentrated sulfuric acid in combination with concentrated nitric acid and $KClO_3$ for the oxidation of graphite for the preparation of graphite oxide. The $KClO_3$ is a highly strong oxidizing agent and it oxidizes the graphite powder in acids solution and typically also is an *in situ* source of dioxygen, which acts as the reactive species. Several research groups have synthesized GO for different application purpose using Hofmann method.[61,62]

2.4. Hummers method: concentrated H_2SO_4 acid in the presence of $KMnO_4$ and $NaNO_3$

In 1958, Hummers and Offeman shows an alternate method for the oxidation of graphite by reacting graphite powder with a mixture of concentrated H_2SO_4, $NaNO_3$ and $KMnO_4$.[28] First graphite powder (100 g) and sodium nitrate (50 g) were stirred in sulfuric acid (2.3 liters) and cooled to 0 °C in ice bath. After that potassium permanganate (300 g) was added to the suspension. During the stirring, the suspension becomes thick and was then further diluted using hot water and treated with H_2O_2 (3%) to reduce the residual permanganate and manganese dioxide to colorless soluble manganese sulfate. Finally, the diluted suspension was filtered and washed several time with warm water to remove the soluble salt of mellitic acid. The dry form of graphitic oxide was obtained by centrifugation followed by dehydration at 40 °C over phosphorus pentoxide in vacuum. In recent time, several research groups have used Hummers improved method for the synthesis of graphite oxide.[10,63–71] All the well known synthesis methods for graphite oxidation using chemical routes have been summarized in Fig. 1.

2.5. Other methods

An improved method for the preparation of graphite oxide was reported by Marcano *et al.*[64] in 2010 (schematic shown in Fig. 2). In this new procedure, the oxidation process was improved by excluding $NaNO_3$, increasing the amount of $KMnO_4$, and performing the reaction in a 9 : 1 mixture of H_2SO_4/H_3PO_4. This improved oxidation method significantly increases the efficiency of graphite oxidation to graphite oxide and also provides a larger amount of graphite oxide as compared to Hummers' method. This oxidation technique also prevented the formation of toxic gases (such as NO_2 and N_2O_4). Another improved synthesis method for large-scale production of graphite oxide involves oxidation of graphite by benzoyl peroxide (strong oxidizer) at 110 °C for 10 min in an opened system.[72] This technique provides a fast and efficient route to GO. Some other oxidizing agents have also been used for the preparation of GO. In this regard, Jone's reagent (H_2CrO_4/H_2SO_4) is also used for the preparation of expanded graphite, which moderately oxidizes graphite.[36] The recent review by Wissler is an excellent, succinct source of further

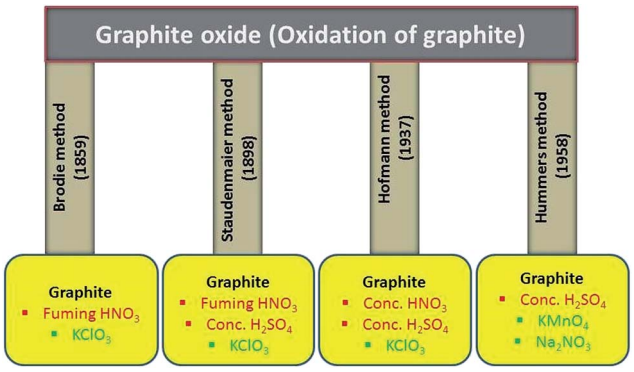

Fig. 1 Methods for synthesis of graphite oxide using graphite, acids and oxidizing chemicals.

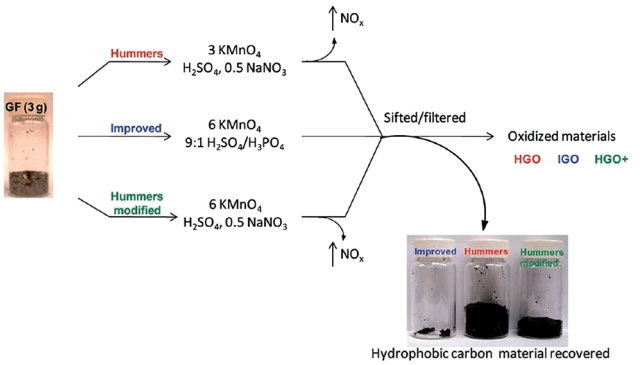

Fig. 2 Representation of the procedures used to form GO starting with graphite flakes. Under-oxidized hydrophobic carbon material recovered during the purification of IGO, HGO, and HGO+. The increased efficiency of the IGO method is indicated by the very small amount of under-oxidized material produced.[64] Reprinted (adapted) with permission from ref. 64. Copyright (2010) American Chemical Society.

information on commonly used graphite and carbons, as well as the terminology used to describe these materials.[73]

3. Functional groups on graphene oxide and its analysis

The structure of GO is described as graphene sheet bonded with several oxygen in the form of hydroxyl, carboxyl, epoxy and others *etc.* groups as shown in Fig. 3.[37] Also, the structure of GO depends significantly on the purification procedures, rather than, as is commonly thought, on the type of graphite used or oxidation protocol.[74] The exact identity and distribution of oxide functional groups depend strongly on the extent of oxidation. The appearance of chemical composition inside GO and the oxygen containing functional groups in GO can be identified using various techniques, including X-ray photoelectron spectroscopy (XPS),[37,75–79] X-ray absorption near-edge spectroscopy (XANES),[71,76,78,80,81] Fourier transform infrared spectroscopy (FTIR),[78,82–84] Raman spectroscopy[79,81,85] and solid-state nuclear magnetic resonance.[37,84,86,87] Mkhoyan *et al.*[41] studied the electronic and atomic structure of GO using dark field imaging of single and multilayer sheets. The results of electron energy loss spectroscopy used for measuring the structure of carbon and oxygen K-edges in a scanning transmission electron microscope indicate the high ratio of sp^3 C–O bonds induces structural distortions. This suggests that the atomic structure of GO sheets should resemble a mostly amorphous 2D sheet of carbon atoms with some of them bonded to oxygen, rather than an ideal sheet of graphene with surface oxidation.

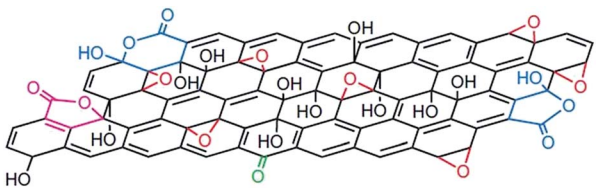

Fig. 3 Structure of GO.[37] Reprinted by permission from Macmillan Publishers Ltd: [Nature chemistry] (ref. 37), copyright (2009).

Functional groups attached on GO surface can also be determined by XPS and it reveals the nature of the carbon and oxygen bonds in their various states as unoxidized carbons (sp^2 carbon), C–O, C═O, and COOH. Several XPS investigation on GO[75,76,88,89] confirms the peaks positions related with different functional groups. The deconvoluted C1s signal of GO, as seen in Fig. 4, composed of mainly five peaks (at room temperature) at different positions corresponding to sp^2 carbons in aromatic rings (284.5 eV) and C atoms bonded to hydroxyl (C–OH, 285.86 eV), epoxide (C–O–C, 286.55 eV), carbonyl (⟩C═O, 287.5 eV), and carboxyl groups (COOH, 289.2 eV). The increase in temperature of GO shows the diminishing of the oxygen containing functional peaks and a very small fraction of C═O peak remains at 1000 °C.[88] The other XPS analysis,[38,81] considered the deconvolution of the C1s spectra using four components, namely, sp^2, C–OH, C–O–C, and COOH, while ignoring the presence of the ⟩C═O groups. In similar way, the deconvolution of the O1s spectra contains the main peaks around 531.08, 532.03, and 533.43 eV and these peaks are assigned to C═O (oxygen doubly bonded to aromatic carbon),[75,82] C–O (oxygen singly bonded to aliphatic carbon), and phenolic (oxygen singly bonded to aromatic carbon)[58,90] groups, respectively. Also pristine GO shows an additional peak at a higher binding energy (534.7 eV).[89]

The XANES is the other powerful characterization tool for the analysis of GO materials. It provides valuable information on the degree of bond hybridization in mixed sp^2/sp^3 bonded carbon, specific bonding configurations of functional atoms, and degree of alignment of the graphitic crystal structures within GO.[76,91]

Raman spectroscopy is an experimental technique that is commonly used to characterize all sp^2 carbons from three to zero dimensions, such as 3D graphite, 2D graphene, 1D carbon nanotubes, and 0D fullerenes.[2] The Raman spectra of GO displays two major D band (1340 cm^{-1}) and a broad G-band at (1580 cm^{-1}).[88] The G-band, which is characteristic of all sp^2-hybridized carbon networks, originates from the first-order scattering from the doubly degenerate E_{2g} phonon modes of graphite in the Brillouin zone center, while the prominent D peak comes from the structural imperfections created by the

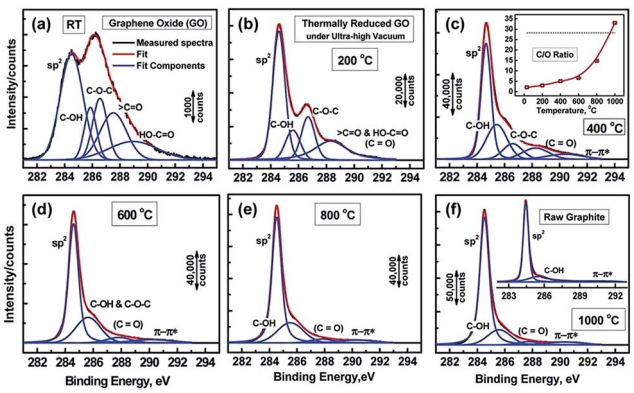

Fig. 4 XPS spectra of GO and oxygen functionalities removal at different temperature.[76] Reprinted (adapted) with permission from ref. 76. Copyright (2011) American Chemical Society.

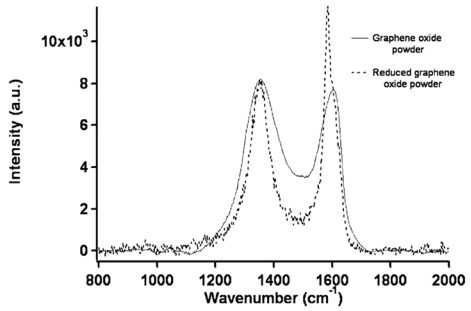

Fig. 5 Raman spectra of the GO and rGO powder.[81] Reprinted (adapted) with permission from ref. 81. Copyright (2009) American Chemical Society.

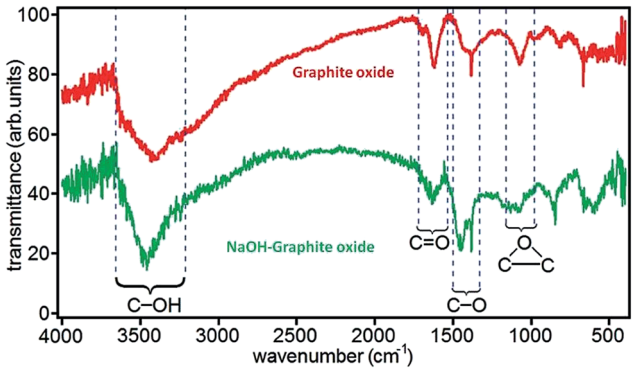

Fig. 6 FTIR spectra of graphite oxide and NaOH–graphite oxide.[78] Reprinted (adapted) with permission from ref. 78. Copyright (2010) American Chemical Society.

attachment of oxygenated groups on the carbon basal plane.[92] Thus, the integrated intensity ratio of the D- and G-bands (I_D/I_G) indicates the oxidation degree and the size of sp^2 ring clusters in a network of sp^3 and sp^2 bonded carbon.[75,92] For example, Mattevi *et al.*,[75] calculated the average graphitic domain size to be ~2.5 nm in pristine GO. Lee *et al.*[81] reported that after thermal reduction of GO, the intensity ration I_D/I_G significantly decreases and this indicates the considerable recovery of the conjugated graphitic framework upon removal of epoxy and hydroxyl groups. Raman spectra in Fig. 5 clearly show that the intensity of G band of rGO is high and sharp as compared to GO.

FTIR spectroscopy is an important tool for characterization of functional groups attached on GO surface. Fig. 6 shows the position of absorption peaks of GO in FTIR and it indicates that different functional groups have different bond energy.[78] In the case of GO, it have different peaks as hydroxyl (broad peak at 3050–3800 cm^{-1}), carbonyl (1750–1850 cm^{-1}), carboxyl (1650–1750 cm^{-1}), C=C (1500–1600 cm^{-1}), and ether or epoxide (1000–1280 cm^{-1}) groups.[78,82,84]

4. Reduction of graphene oxide

4.1. Chemical reduction

Chemical reduction of graphite oxide is one of the excellent procedures to synthesized rGO and graphene in large quantities.[28,93,94] It includes ultrasonication of graphite oxide in water forming a homogeneous dispersion of predominantly soluble GO in water. The GO is reduced by a suitable chemical process; the reduced GO formed resembles graphene but contains residual oxygen and other hetero atoms, as well as structural defects. During the reduction processes, most oxygen-containing functional groups of GO are eliminated and the π-electron conjugation within the aromatic system of graphite is partially restored. Finally the rGO gets precipitated from the reaction medium because of the recovered graphite domains of chemically converted graphene sheets with increased hydrophobicity and π-stacking interaction.[95] The properties of rGO are nearly similar to that of graphene prepared through different chemical, thermal, photo, electrochemical or microwave reduction pathways.[36] The most widely applied technique used for preparing chemically converted reduced GO is the chemical reduction of GO as shown in Fig. 7.[96]

Shin *et al.*[97] used $NaBH_4$ for the reduction of graphite oxide. The different molar concentrations of $NaBH_4$ shows different order of reduction confirmed by XRD patterns and it also shows enhanced electrical properties after reduction. Fig. 8 shows the XRD pattern of graphite oxide after reduction by $NaBH_4$ which clearly shows the shifting and broadening of peaks at different molar concentrations of $NaBH_4$. At higher $NaBH_4$ molar concentrations (150 mM), the peak of the large interlayer distance disappeared and shifted into a broad peak near $2\theta = 23.98$. This implied that functional groups were removed.

Fan *et al.*[98] reported that the exfoliated graphite oxide can undergo quick deoxygenation in strong alkali solutions like NaOH and KOH at moderate temperatures (50–90 °C) resulting in stable aqueous graphene suspensions. Fig. 9 shows that the addition of NaOH to the graphite oxide suspension led to the change in color (yellow-brown to dark black).

Various inorganic and organic reducing agents such as phenyl hydrazine,[99] hydrazine hydrate,[95] sodium borohydride,[97,100] ascorbic acid,[101,102] glucose,[103] hydroxylamine,[104] hydroquinone,[105] pyrrole,[106] amino acids,[107,108] strongly alkaline solutions[98] and urea[109] have been explored for the chemical

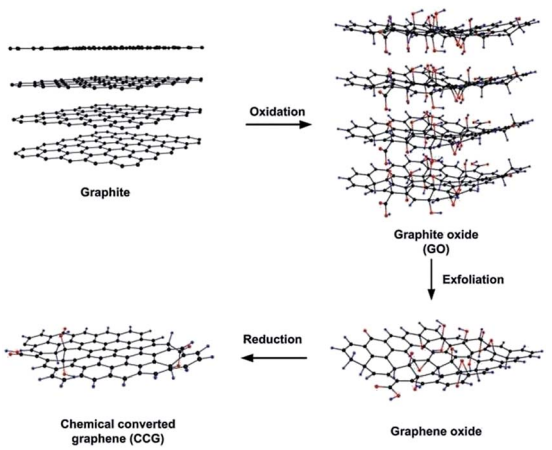

Fig. 7 Preparation of chemically converted graphene (CCG) by reduction of GO.[96] Reprinted (adapted) with permission from ref. 96. Copyright © 2011 WILEY-VCH Verlag GmbH & Co. KGaA, Weinheim.

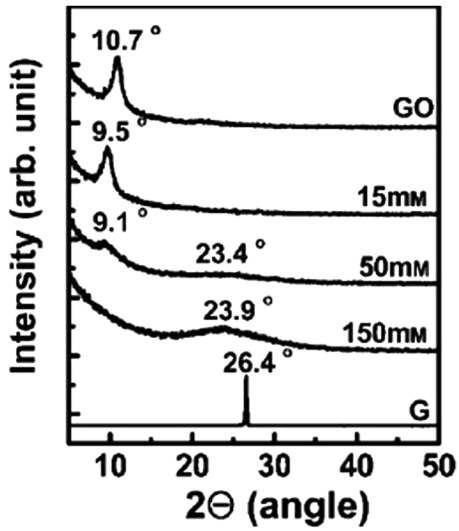

Fig. 8 XRD patterns of GO, graphite (G), and rGO obtained using various molar concentrations of $NaBH_4$.[97] Reprinted (adapted) with permission from ref. 97. Copyright © 2009 WILEY-VCH Verlag GmbH & Co. KGaA, Weinheim.

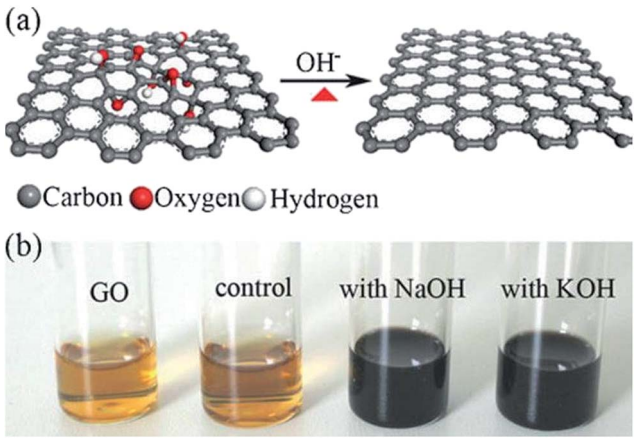

Fig. 9 (a) Illustration for the deoxygenation of exfoliated graphite oxide under alkaline conditions and (b) images of the exfoliated-graphite oxide suspension (~0.5 mg mL^{-1}) before and after reaction. The control experiment in (b) carried out by heating the pristine exfoliated-graphite oxide suspension without NaOH and KOH at 90 °C for 5 h with the aid of sonication.[98] Reprinted (adapted) with permission from ref. 98. Copyright © 2008 WILEY-VCH Verlag GmbH & Co. KGaA, Weinheim.

reduction of GO. Wang *et al.* reported that high-temperature alcohol vapor can also be used as an effective reducing agent of GO and the resulting chemically converted reduced graphene exhibits a highly graphitic structure and excellent electrical conductivity.[105]

4.2. Thermal reduction

Thermal reduction of GO or graphite oxide is an important processing step in the synthesis of many graphene-based materials and devices. The GO reduced by heating is known as thermal reduction by annealing. Annealing atmosphere is also important for the reduction of GO. Annealing reduction is usually carried out in vacuum,[110] or in inert[111] or reducing atmosphere.[111–113] Thermal reduction of GO comprised of the thermal-energy-induced multistep removal of intercalated H_2O molecules and oxide groups of carboxyl, hydroxyl, and epoxy. It should be noted that in chemical reduction, individual GO sheets in the solution phase are chemically reduced by the strong chemical base.[114] The rapid heating of graphite oxide at high temperature, exfoliates in the form of porous carbon materials and get converted into graphene with fewer amounts of oxygen functionalities. The exfoliation occurs by the sudden expansion of CO or CO_2 gases evolved from the spaces between graphene sheets during rapid heating of the graphite oxide. The rapid heating makes the oxygen containing functional groups attached on carbon plane to decompose into gases that create huge pressure between the stacked carbon layers. Based on state equation, a pressure of 40 MPa is generated at 300 °C, while 130 MPa is generated at 1000 °C.[115] The evaluation of the Hamaker constant predicts that a pressure of only 2.5 MPa is enough to separate two stacked GO platelets.[115] Rapid heat treatment at elevated temperature, not only exfoliate graphite oxide but also reduce the functionalities by decomposing oxygen containing groups. The notable effect found during the thermal exfoliation is the structural defect and damage of graphene sheets caused by the release of carbon dioxide.[90] These structural defects and damage inevitably affect the electronic properties by decreasing the ballistic transport path length and introducing scattering centers.

The heating temperature severely affects the removal of oxygen from GO surfaces and consequently effect the reduction of GO.[90,110,111] Li *et al.*[112] monitored the variation of chemical structure with annealing temperature, and concludes that the high temperature is needed to achieve the better reduction of GO. Schniepp *et al.*[90] reported the C/O ratio less than 7 for heating temperature less than 500 °C, and its ratio increases to higher than 13 as the heating temperature reaches to 750 °C. The reduction of GO usually enhances the electrical conductivity due to the removal of oxygen containing groups. Wang

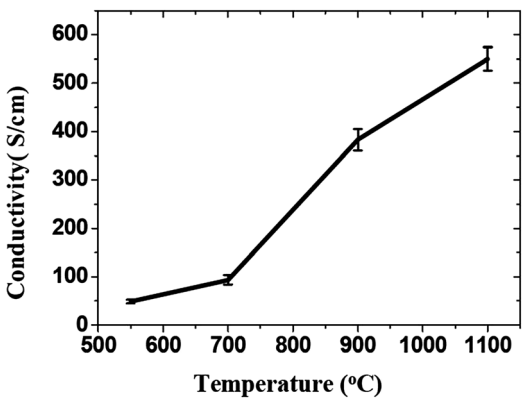

Fig. 10 Increase of the average conductivity of graphene films with temperature.[111] Reprinted (adapted) with permission from ref. 111. Copyright (2008) American Chemical Society.

et al.[111] found the conductivity of GO thin films to increases with annealing temperature as shown in Fig. 10. Electrical conductivity of the reduced GO film obtained at 550, 700, 900 and 1100 °C were 49, 93, 383 and 550 S cm^{-1}, respectively. Wu *et al.*[113] reported the hydrogen arc-discharge exfoliation technique for exfoliation of graphite oxide to prepare graphene. Since the arc-discharge could provide temperatures above 2000 °C in a short time and the electrical conductivity of graphene sheets was found to be 2000 S cm^{-1}.

4.3. Microwave and photo reduction

Microwave heating is widely used for the exfoliation and reduction of graphitic precursor materials. With microwave treatments, the preparation of graphene can be performed by solid-state reduction of dry graphite oxide, the reduction of graphite oxide in suspension, or by heating graphite intercalated compounds (GICs). Furthermore, the simultaneous reduction and doping of GO and the preparation of hybrid materials is also possible. The GO synthesis and reduction using unconventional heating like microwave-irradiation (MWI)[116–118] and photo-irradiation[119,120] is a fast and energy-efficient method. MWI induced heating has been used as a rapid way to synthesize graphene sheets.

Microwave assisted heating can provide significant enhancement in the transfer of energy directly to the reactants which causes instantaneous rise in internal temperature.[118,121] The rise in instantaneous internal temperature can shorten the reaction time significantly, and improves the reaction efficiency. Also, owing to the difference in the solvent and reactant dielectric constants, selective dielectric heating provides significant enhancement in the direct energy transfer to the reactants, which causes an instantaneous internal temperature rise and thereby reduction of GO.[118] Dry GO absorbs MWI strongly with a sudden increase in surface temperature up to ~400 °C, of the GO, within just 2 s, leading to an ultrafast reduction of GO to rGO.[103] Several research groups have used MWI for the synthesis as well as reduction of GO.[117,122–126] Zhu *et al.*[117] reported a simple and versatile method to simultaneously achieve the exfoliation and reduction of graphite oxide within 1 min by treating graphite oxide powders in a commercial microwave oven. Yan *et al.*[127] described a new approach for the reduction of GO using glucose in an alkaline environment by microwave heating. Chen *et al.*[128] reduces GO in a mixed solution of *N*,*N*-dimethylacetamide and water (DMAc/H_2O). The mixed solution works both as a solvent for the production of graphene and as a medium to control the temperature of the reactive system up to 165 °C. Here the reduction of GO can be accomplished in time scale of minutes, and the degree of reduction depends on the duration of microwave treatment and given power (800 W). Fig. 11 shows the optical image of GO suspension with concentration of 0.56 mg mL^{-1} in water or DMAc/water mixture before and after microwave heating for different times. At first, an aqueous suspension of GO is yellow-brown in color and after microwave irradiation for different time duration its color starts to change and finally changes to black. The GO suspension exhibited long-term stability at room temperature without precipitation.

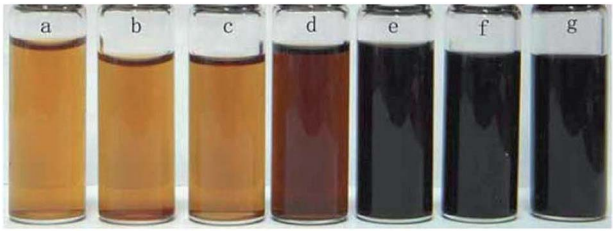

Fig. 11 Photographs of GO suspension with concentration of 0.56 mg mL^{-1} (a–f) under different conditions. (a) GO aqueous suspension after microwave treatment for 1 min, (b) GO suspension in DMAc/H_2O (6 : 1), (c–f) GO suspension in DMAc/H_2O (6 : 1) after microwave treatment for 1, 2, 3, and 10 min (2 min × 5 times), respectively, (g) re-dispersed of the dried graphene into pure DMAc with concentration of 1.0 mg mL^{-1}.[128] Reprinted (adapted) with permission from ref. 128. Copyright © 2010 Elsevier B. V. All rights reserved.

Photo reduction like photo-thermal and photo-chemical reduction of GO is a additive free, facile, clean, and versatile approach to reduce GO. High-quality rGO has been prepared by irradiating GO with sunlight, ultraviolet light, and KrF excimer laser.[129] Ding *et al.*[130] reduced GO using UV irradiation to obtain single to few-layered graphene sheets without the use of any photocatalyst. Cote *et al.*[120] prepared rGO by photothermal reduction of GO using xenon flash at ambient conditions and patterned GO or GO/polymer films using photomask. Nanosecond laser pulses of KrF eximer laser of 335 and 532 nm effectively reduces dispersed GO to thermally and chemically stable graphene.[131] Photochemical reduction of GO to graphene has also been exploited for patterning. The photo-reduction and patterned film fabrication was carried out with femto-second laser irradiation.[119] The focused laser beam (laser pulse of 790 nm central wavelength, 120 fs pulse width, 80 MHz repetition rate, focused by a ×100 objective lens) was used to heat the

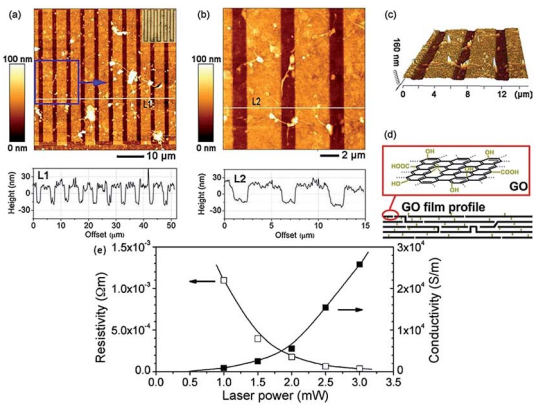

Fig. 12 (a) AFM image of comb-like microcircuit and height profile along the white line (L1), inset is the optical micrograph of the microcircuit; (b) magnified image of the local pattern (blue square of a) and height profile along the white line (L2); (c) 3D image of (b); (d) illustration for the profile of GO film before and after femto second laser reduction and (e) dependence of resistivity and conductivity of reduced and pattern GO micro-belts on laser power.[119] Reprinted (adapted) with permission from ref. 119. Copyright © 2005 Elsevier B. V. All rights reserved.

localized GO film with a line width in the range of 1.5 μm. As a result, the laser reduction can produce rGO films with a much higher conductivity with laser incident power by laser writing as shown in Fig. 12.

Supported GO films on different substrates were also irradiated by excimer laser for its reduction. GO film deposited on Si substrates were subjected to excimer laser radiation (Lambda Physik KrF excimer laser, 248 nm wavelength, 30 ns lifetime, 300 mJ laser energy, 5 Hz repetition rate, 200 shots), for reduction and patterning.[132,133] The high energy direct electron-beam is also capable for the reduction of GO.[134] The GO can be reversibly reduced and oxidized using electrical stimulus. Controlled reduction and oxidation in two-terminal devices containing multilayer GO films was demonstrated by Ekiz *et al.*[135] and Yao *et al.*[136]

4.4. Photo catalyst reduction

The review article published by Pei *et al.* gives a detailed overview and description about the reduction of GO by photocatalysis method.[94] The attached functional groups on GO surfaces can be removed by the help of photocatalyst like TiO_2 which turns it into reduced GO. Kamat research group[137] reported the reduction of GO in a colloidal state with the help of TiO_2 nanoparticles under ultraviolet irradiation. The GO suspended in ethanol undergoes reduction as it accepts electrons from UV-irradiated TiO_2 nanoparticles suspensions. After reduction through TiO_2 photo catalyst, the color of the GO suspension changes from brown to black as shown in Fig. 13. Also the photocatalytic properties of semiconducting TiO_2 particles have been thoroughly investigated.[138] In the presence of ethanol the holes are scavenged to produce ethoxy radicals, thus leaving the electrons to accumulate within the TiO_2 particles. The accumulated electrons interact with GO sheets to reduce functional groups and before reduction, the carboxyl groups in GO surface can interact with the hydroxyl groups on the TiO_2 surface by charge transfer mechanism, producing a hybrid connection between TiO_2 and the GO, and this structure can be retained after reduction. The rGO sheets can work as a current collector to facilitate the separation of electron/hole pairs in some photovoltaic devices like photocatalysis device[139] and in dye-sensitized solar cell.[140,141] The similar reduction mechanism has also been found in other carbon materials such as carbon nanotubes and fullerene.[142,143] Beyond TiO_2, different materials with photo catalytic activity, like $BiVO_4$ (ref. 128) and ZnO[144] have also been reported to achieve the reduction of GO.

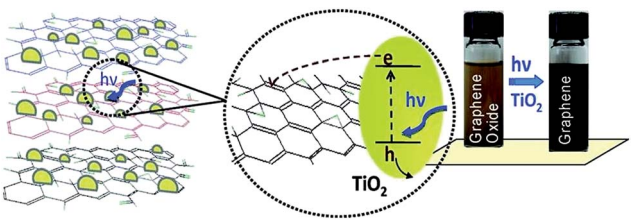

Fig. 13 Photo catalyst electron acceptance by GO and change in color from brown to black after GO reduction.[137] Reprinted (adapted) with permission from ref. 137. Copyright (2008) American Chemical Society.

4.5. Solvothermal/hydrothermal reduction

The reduction of GO through solvothermal or hydrothermal route generally occurs at low temperature and high pressure is also an important series in the field of graphene synthesis and reduction.[145–147] Solvothermal processes can be defined as chemical reactions or transformations in a solvent under supercritical conditions or near by pressure–temperature domain resulting from heating.[148] Inside the sealed container, the reduction occurs through processes involving surface chemistry, the reactivity being increased under high pressure conditions and at moderate temperatures. The hydrothermal method has been applied for the transformation of carbohydrate molecules to form homogeneous carbon nano-spheres[149] and nanotubes.[150] Zhou *et al.*[147] reported that supercritical water plays the role of reducing agent in hydrothermal conditions and offers green chemistry alternative to organic solvents. This result shows that the supercritical water removes the functional groups attached on GO and also recovers the aromatic structures of carbon lattice. Fig. 14 shows that after reduction the solution color changes from brown to dark black and UV visible absorption shows the decrease in band gap after reduction of GO.

Wang *et al.*[146] employed *N*,*N*-dimethylformamide as solvent for the reduction of GO using solvothermal method. After solvothermal treatment (180 °C for 12 h) the C/O ratio of rGO is higher than that produced by hydrazine reduction at normal pressure. It reveals that more oxygen content was removed after the solvothermal treatment. Dubin *et al.*[145] proposed a modified solvothermal reduction method using *N*-methyl-2-purrolidinone (NMP) as solvent. This treatment was not performed in a sealed container and the heating temperature was lower than the boiling point of NMP. As a result, there is no additional pressure present

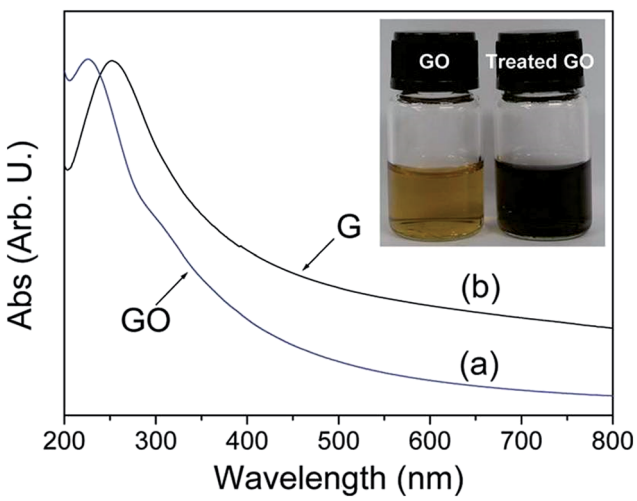

Fig. 14 UV visible absorption spectra of the GO (a) before and (b) after hydrothermal treatment at 180 °C for 6 h. Inset shows the color change of 0.5 mg mL^{-1} GO solution before and after hydrothermal treatment.[147] Reprinted (adapted) with permission from ref. 147. Copyright (2009) American Chemical Society.

Table 1 Reduction approach of GO using reducing chemical agents with different conditions

Reducing chemical agents/method	Temp. (°C)	Time (h)	Solvent	O content (at%)/C/O atomic ratio*	Ref.
N_2H_4 + NH_3 solution	95	1	H_2O	—	151
N_2H_4/DMF	180	12	DMF	1.5	146
Ascorbic acid	RT	48	H_2O	—	101
Hexamethylenetetramine	RT	12	H_2O	—	152
S-Containing compound	95	3	H_2O/DMAc–H_2O	6.48*	153
Glucose + ammonia solution	95 (RT)	1 (48)	H_2O	—	154
Hydrazine hydrate	100	24	H_2O	10.3*	95
Fe powder	RT	6	H_2O	7.9*	155
Zn + H_2SO_4	RT	2	H_2O	4.5	156
Hydroquinone	Refluxed	20	H_2O	—	105
$NaBH_4$	125	3	H_2O	—	72
Tellurium nanowire	RT	36	H_2O	—	157
Ascorbic acid + amino acid	80	24	H_2O	—	107
Solvothermal reduction	205	24	NMP	13.8	145
Solvothermal reduction	120–200	4–48	H_2O, ethanol, 1-butanol, ethelene glycol	6.6–16.6	158
Thermal reduction	150	8	DMAc + H_2O	4.7*	159

in the reduction process. The C/O ratio of the solvothermal rGO is very low (5.15) and this reduction method can only achieve a moderate reduction of GO. The electrical conductivity of the rGO films achieved by this solvothermal reduction and subsequent vacuum filtration is 3.74×10^2 S cm^{-1}, which is one order of magnitude smaller than that produced by hydrazine reduction (8.28×10^3 S cm^{-1}).

Various research groups have shown the reduction of GO using different chemical agents with different solvent, at different temperatures and time as summarised in Table 1.

5. Frontier applications of graphene oxide

5.1. Lithium ion battery application

5.1.1. Anode materials. Zhu *et al.*[160] utilized microwave irradiation to yield rGO platelets decorated with Fe_2O_3 nanoparticles and used it as an anode material for Li-ion batteries which exhibited discharge and charge capacities of 1693 and 1227 mA h g^{-1}, respectively, normalized to the mass of Fe_2O_3 in the composite (and ~1355 and 982 mA h g^{-1}), respectively. A three-layer-structured hybrid nanostructure consisting of transition metal oxide TiO_2 nanoparticles sandwiched between carbonaceous polymer polyaniline and graphene nanosheets enabled fast discharge and charge comparison to TiO_2 as reported by Zhang *et al.*[161] Wang *et al.*[162] reported the adaptable silicon–carbon nanocables sandwiched between reduced GO sheets as a anode material for lithium ion battery. This electrode exhibited reversible specific capacity of 1600 mA h g^{-1} at 2.1 A g^{-1}, 80% capacity retention after 100 cycles, and superior rate capability (500 mA h g^{-1} at 8.4 A g^{-1}) on the basis of the total electrode weight. Poly(3,4-ethylenedioxythiophene) sheath over a SnO_2 hollow spheres/GO hybrid worked as a durable anode in Li-ion batteries.[163] Few-layer reduced GO synthesized in GO solution using EDA as a reducing agent and a cross-linker were utilized as a electrode material in lithium ion battery.[164] CoO hollow cube/rGO composites enhances the lithium storage capability,[164] whereas $CoMoO_4$ nanoparticles anchored on reduced GO nanocomposites enhanced the cyclic stability of anodes for lithium-ion batteries.[165] Germanium nanoparticles encapsulated in nitrogen-doped reduced GO were also utilized as an advanced anode material for lithium-ion batteries by Yan Xu *et al.*[166] The Ge/rGO composite exhibited an initial discharge capacity of 1475 mA h g^{-1} and a reversible capacity of 700 mA h g^{-1} after 200 cycles at a current density of 0.5 A g^{-1}. Moreover, Ge/rGO showed a capacity of 210 mA h g^{-1} even at a high current density of 10 A g^{-1}. Zhang *et al.*[167] proposed a facile, low-cost and scalable thermal annealing method for the synthesis of phosphorus-doped graphene (PG) using graphite oxide (GO) and triphenylphosphine (TPP) as carbon and phosphorus sources, respectively. The resultant PG exhibited enhanced electrochemical properties as an anode material in LIBs comparison to undoped graphene.

Anode based on hydrogen-enriched reduced GO showed an enhanced electrochemical performance as reported by Yoon *et al.*[168] A sandwiched nano-architecture of rolled-up Si/reduced GO bilayer nano-membranes was utilized as anodes for lithium-ion batteries, which demonstrated long cycling life of 2000 cycles at 3 A g^{-1} with a capacity degradation of only 3.3% per 100 cycles.[169] Zeng *et al.*[170] presented a facile approach to fabricate flexible spinel-type oxide/reduced GO composite aerogels as binder-free anodes. Gao *et al.*[171] reported a multi-layered structural silicon-reduced GO electrode which showed a stable charge–discharge performance with high rate, a reversible capacity of 2787 mA h g^{-1} at a charging rate of 100 mA g^{-1}, and a stable capacity over 1000 mA h g^{-1} retained at 1 A g^{-1} after 50 cycles. The cycling performance and columbic efficiency of the Si/rGO anode are shown in Fig. 15a. Fig. 15b and c shows galvanostatic cycling and the rate capability respectively.

Besides various rGO based composites like (i) crumpled rGO/MoS_2 nanoflowers,[172] (ii) amorphous GeO_x-coated rGO balls,[173]

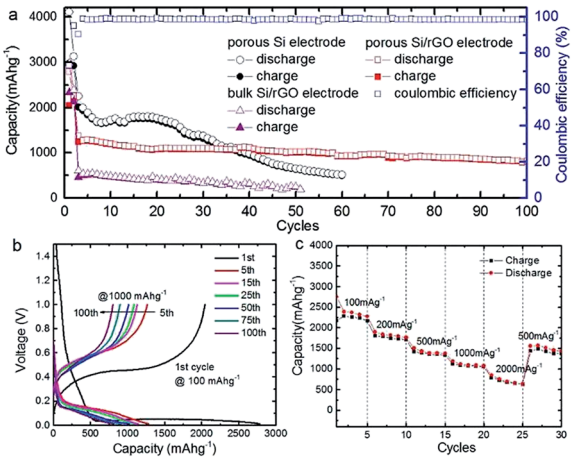

Fig. 15 (a) Cycle performance at a constant current rate of 1000 mA g^{-1} after initial activation processes at 100 mA g^{-1} for two cycles; (b) galvanostatic discharge–charge profiles; and (c) rate performance of Si/graphene composite electrode.[171] Reprinted (adapted) with permission from ref. 171. Copyright (2015) American Chemical Society.

(iii) copper sulfide nanowires/rGO,[174] (iv) Si/Ti_2O_3/rGO,[175] (v) MnS hollow microspheres-rGO,[176] (vi) copper silicate hydrate hollow spheres-rGO[177] (vii) fluorine-doped tin oxide nanocrystal/rGO,[178] (viii) hollow nanobarrels of α-Fe_2O_3 on rGO[179] and (ix) hierarchical rGO-$Co_2V_2O_7$ nanosheets[180] *etc.* shows an improved performance and stability as anode material for the lithium-ion batteries.

5.1.2. Cathode materials. Ha *et al.*[181] reported the fabrication and electrochemical activity of free-standing reduced GO films as cathode materials for lithium ion batteries. The conducting additive and binder-free rGO electrodes with different oxygen contents were assembled by a simple vacuum filtration process from aqueous rGO colloids prepared with the aid of cationic surfactants. The gravimetric capacity of rGO film cathodes showed clear dependence on the oxygen contents controlled by the thermal reduction process. The capacity increased with the increase of the amount of oxygen functional groups. Guo *et al.*[182] prepared a GO/$LiFeSO_4F$ composite which served as a cathode material for improved cycle stability and rate capability of for lithium-ion batteries. This unique structure constructs an effective electronic conductive network, thus reducing the inner resistance of the battery, facilitating the charge transfer reactions at the electrode/electrolyte interface, and improving the lithium diffusion in the electrode bulk.

5.1.3. Lithium–sulfur battery. Lithium–sulfur batteries hold great promise for serving as next generation high energy density batteries. However, the shuttle of polysulfide induces rapid capacity degradation and poor cycling stability of lithium–sulfur cells. Since the loss of sulfur cathode material as a result of polysulfide dissolution causes significant capacity fading in rechargeable lithium/sulfur cells. Ji *et al.*[183] used a chemical approach to immobilize sulfur and lithium polysulfides *via* the reactive functional groups on GO. Strong interaction between GO and sulfur or polysulfides enabled lithium/sulfur cells with a high reversible capacity of 950–1400 mA h g^{-1}, and stable cycling for more than 50 deep cycles at 0.1C (1C = 1675 mA g^{-1}). An amylopectin wrapped GO–sulfur composite was prepared by W. Zhou *et al.* to construct a 3-dimensionally cross-linked structure through the interaction between amylopectin and GO, for stabilizing lithium sulfur batteries.[184] With the help of this cross-linked structure, the sulfur particles get confined among the layers of GO and exhibited significantly improved cyclability, compared with the unwrapped GO–sulfur composite.

A generic method of coating GO on particles by engineering the ionic strength of solutions was developed by Rong *et al.*[185] Uniform coating of GO on various particles with a wide range of sizes, geometries, and compositions were achieved. GO on sulfur particles to form sulfur/GO core–shell particles as Li–S battery cathode materials was investigated, and found that the sulfur/GO composite material exhibits significant improvements in electrochemical performance over sulfur particles without coating. The optical images and charge discharge curves of the sulfur/GO are shown in the Fig. 16.

Since lithium sulfide (Li_2S) is a promising cathode material for Li–S batteries with high capacity (theoretically 1166 mA h g^{-1}) and can be paired with non lithium–metal anodes to avoid potential safety issues. However, the cycle life of coarse Li_2S particles suffers from poor electronic conductivity and polysulfide shuttling. Wang *et al.*[186] developed a flexible slurryless nano-Li_2S/reduced GO cathode paper which was directly used as a free-standing and binder-free cathode without metal substrate. It showed an excellent rate capability and cycle life. Hwa *et al.*[187] also reported the lithium sulfide/GO nanospheres with conformal carbon coating as a high-rate, long-life cathode for Li/S cells. Huang *et al.*[188] proposed a unique lithium sulfur battery configuration with an ultrathin GO membrane for high stability.

5.1.4. Lithium oxygen battery. Lithium–oxygen batteries as electrical energy storage are attractive with exceptionally high-energy density but endure from small rate capability, poor cyclic stability and a scarcity of steady electrolytes. Ruthenium-based nanomaterials supported on rGO were tested as a catalysts for the oxygen reduction (ORR, Li_2O_2 formation) and

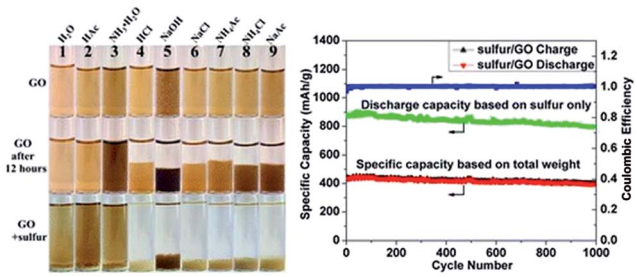

Fig. 16 Digital images of GO dispersed in different solutions at the beginning, after 12 h and after adding sulfur particles to GO dispersion. Galvanic charge–discharge performance and coulombic efficiency of sulfur/GO at 1 A g^{-1} for 1000 cycles. Discharge specific capacity calculated based on weight of sulfur only (green dotted line) and total weight of sulfur/GO are plotted.[185] Reprinted (adapted) with permission from ref. 185. Copyright (2014) American Chemical Society.

oxidation (OER, Li_2O_2 reconversion) in the Li/O_2 cells using a TEGDME-$LiCF_3SO_3$ electrolyte by Jung *et al.*[189]. Sun *et al.*[91] reported the synthesis of porous graphene with different pore size architectures as cathode catalysts for Li–O_2 batteries. The addition of ruthenium (Ru) nanocrystals to porous graphene promotes the oxygen evolution reaction. The Ru nanocrystal-decorated porous graphene exhibited an excellent catalytic activity as cathodes in Li–O_2 batteries with a high reversible capacity of 17 700 mA h g^{-1}, a low charge/discharge overpotential (about 0.355 V), and a long cycle life up to 200 cycles (under the curtaining capacity of 1000 mA h g^{-1}).[91] Nanocrystalline Co_3O_4, grown on reduced graphene oxide (Co_3O_4/RGO) was employed as part of a carbon-based oxygen electrode membrane which results in significant reduction of overpotentials for OER (up to 350 mV), and improved cycling performance in the Li–O_2 cell.[190] Li *et al.*[191–193] employed pure, nitrogen and sulphur doped graphene nano sheets derived from the thermal reduction of GO in lithium–oxygen batteries and found that they show excellent electrocatalytic activity for oxygen reduction.

5.2. Solar cell applications

Organic photovoltaic (OPV) materials have recently garnered significant attention as enablers of high power conversion efficiency (PCE), low-cost, mechanically flexible solar cells. Nevertheless, further understanding-based materials developments will be required to achieve full commercial viability. In particular, the performance and durability of many current generation OPVs are limited by poorly understood interfacial phenomena.

The utilization of GO thin films as the hole transport and electron blocking layer in organic photovoltaics was demonstrated by Li *et al.*[194] The incorporation of GO deposited from neutral solutions between the photoactive poly(3-hexylthiophene) (P3HT):phenyl-C_{61}-butyric acid methyl ester (PCBM) layer and the transparent and conducting indium tin oxide led to a decrease in recombination of electrons–holes and leakage currents. This resulted in a dramatic increase in the OPV efficiencies to values that are comparable to devices fabricated with PEDOT:PSS as the hole transport layer. Liu *et al.*[195] utilized sulfated GO as a hole-extraction layer for high-performance polymer solar cells. Radich *et al.*[196] reported Cu_2S reduced GO composite for high-efficiency quantum dot solar cells.

Murray *et al.*[197] applied electronically tuned GO as an effective interfacial layer (IFL) for templating the optimum donor polymer π-stacking orientation for high efficiency OPVs. In addition to functioning as a solution-processable PEDOT:PSS alternative, GO significantly enhances the durability of fully fabricated devices by increasing the active layer-IFL interfacial stability under thermal and environmental stress.

Kavan *et al.*[198] used optically transparent cathode for Co(III/II) mediated dye-sensitized solar cells (DSSC) based on GO. Various other counter electrodes like (i) rGO–TaON composite for $Co(bpy)_3^{3+/2}$ mediated DSSC,[199] (ii) multiwalled carbon nanotube@rGO nanoribbon,[200] (iii) TiO_2 photo-anodes with nitrogen–rGO,[201] (iv) rapid atmospheric pressure plasma jet processed rGO,[202] (v) nanocomposite of tin sulfide nanoparticles with rGO,[203] and (vi) GO assisted anatase TiO_2 nanosheets[204] were utilized to improve the overall performance and efficiencies of the solar cells. Han *et al.*[205] reported rGO/mesoporous–TiO_2 nanocomposite based meso-structured perovskite solar cells that showed an improved electron transport property owing to the reduced interfacial resistance. This effect significantly increased the short circuit current density and open circuit voltage. The rGO/mesoporous–TiO_2 nanocomposite film with an optimal rGO content of 0.4 vol% shows 18% higher photon conversion efficiency compared with the TiO_2 nanoparticles based perovskite solar cells.

5.3. Supercapacitor applications

An alternative and effective route to prepare conducting polyaniline-grafted rGO composite with highly enhanced properties was reported by Kumar and co-workers.[206] The composite showed more pronounced electrochemical performances than the pristine GO as supercapacitor electrodes, exhibiting a capacitance value of 250 F g^{-1}. Xu *et al.*[207] prepared GO (GO)/polyaniline nanocomposite by *in situ* polymerization with the assistance of supercritical carbon dioxide (SC CO_2) which exhibited high specific capacitance (425 F g^{-1}) at a current density of 0.2 A g^{-1}. A hierarchical high-performance electrode with nanoacanthine-style polyaniline deposited onto a carbon nanofiber/GO template was successfully prepared by Xu *et al.*[208] *via in situ* polymerization process. The hierarchical free-standing electrodes showed a significant specific capacitance of 450.2 F g^{-1} at the voltage scan rate of 10 mV s^{-1}.

Zhang *et al.*[209] developed a highly conductive, free-standing, and flexible porous carbon film by simple KOH activation of reduced G-O films. The supercapacitors constructed with these films as electrodes yielded outstanding power and frequency performance, simultaneously maintaining excellent energy densities. Li *et al.*[210] prepared hierarchical flowerlike NiO/reduced GO composites which showed a maximum specific capacitance ~428 F g^{-1} at a discharge current density of 0.38 A g^{-1} in a 6.0 M KOH electrolyte.

Hsieh *et al.*[211] reported high specific capacitance, superior rate capability, and excellent cyclic stability of reduced GO nanosheets decorated with SnO_2 nanocrystals as electrode materials for electrochemical capacitors. Xing *et al.*[212] reported a facile photochemical reduction method for producing the photoreduced graphene hydrogels with 3D porous structures from GO suspension. The supercapacitor based on this structure performed a high specific capacitance of 254 F g^{-1} at 1 A g^{-1} in KOH electrolyte. Sahu *et al.*[213] synthesized high performance lacey rGO nanoribbons (LrGONR). Holes created during the LrGONR synthesis not only enhanced the electrolytic accessibility but destacked all the graphene layers through protrusion at edge planes and corrugation in individual graphene. The supercapacitor exhibited exceptionally high energy/power density, typically 15.06 W h kg^{-1}/807 W kg^{-1} in aqueous at 1.7 A g^{-1}, 90 W h kg^{-1}/2046.8 W kg^{-1} in non aqueous at 1.8 A g^{-1}, and 181.5 W h kg^{-1}/2316.8 W kg^{-1} in ionic electrolyte at ~1.6 A g^{-1}.

A ternary nanocomposite system, composed of poly(-vinylidene fluoride) (PVDF), NH_2-treated graphene nanodots (GND), and rGO, was synthesized by Sunghun Cho *et al.*[214] The resulting PVDF/NH_2 treated GND/rGO nanocomposite exhibited higher dielectric constant ($\varepsilon' \approx 60.6$) and larger energy density ($U_e \approx 14.1$ J cm^{-3}) compared with the pristine PVDF ($\varepsilon' \approx 11.6$ and $U_e \approx 1.8$ J cm^{-3}).

Kumar *et al.*[55,190–193,215] synthesized different graphene–metal oxide based hybrid materials as electrodes for supercapacitor applications. The reported work shows that the electrochemical performance of a interesting three-dimensional structures comprised of zero-dimensional cobalt oxide nanobeads, one-dimensional carbon nanotubes and two-dimensional graphene, stacked hierarchically.[215] The electrode based on this hierarchical structure showed an electrochemical performance with a maximum specific capacitance of 600 F g^{-1} at the charge/discharge current density of 0.7 A g^{-1} in KOH electrolyte. An ultrathin supercapacitor electrode was fabricated by solution-processable assembly of rGO nanosheets with a photo-cross-linkable polymer by Jo *et al.*[216] UV treatment triggered cross-linking of DR with PEDOT:PSS, causing pure electrostatic interactions to convert to covalent bonds. This film exhibited a large volumetric capacitance value of 354 F cm^{-3}.

Three dimensional rGO/Ni foam composites were prepared by Yang *et al.*[217] by reduction of GO by Ni foam directly in its aqueous suspension at pH 2 at room temperature. When the reduction time increased from 3 to 15 days, the areal capacitance of the composite increases from 26.0 to 136.8 mF cm^{-2} at 0.5 mA cm^{-2}. The 5 h rGO/Ni foam composite shows an areal capacitance of 206.7 mF cm^{-2} at 0.5 mA cm^{-2} and good rate performance and cycling stability with areal capacitance retention of 97.4% after 10000 cycles at 3 mA cm^{-2}. Further extending the reduction time to 9 h at 70 °C, the composite shows a high areal capacitance of 323 mF cm^{-2} at 0.5 mA cm^{-2}. Fig. 17a shows the digital image of Ni foams before and after 7 day immersion in the GO aqueous suspension with different pH values. The microstructures of pristine Ni foam and the rGO/Ni foam composite prepared at pH-2 for 7 days are shown in Fig. 17b–d.

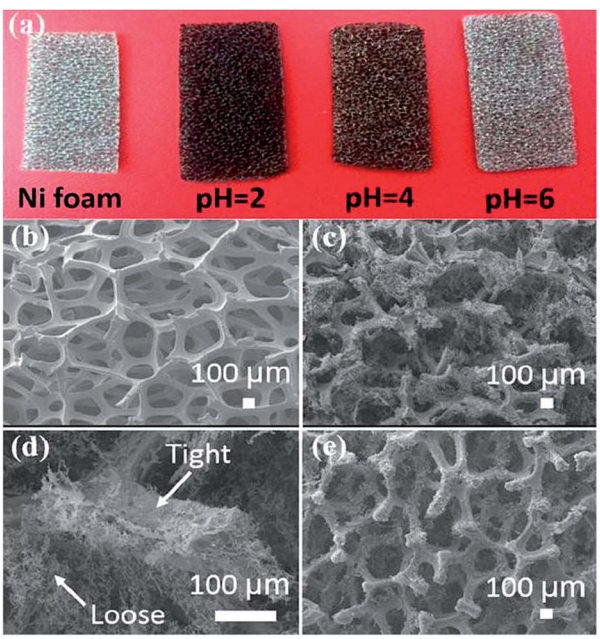

Fig. 17 (a) Digital image of pristine Ni foam and the Ni foams after immersion in GO suspensions with different pH values for 7 days of reduction at room temperature. SEM images of (b) pristine Ni foam, (c, d) freeze-dried 7 day rGO/Ni foam composite, and (e) freeze-dried 3 day rGO/Ni foam composite.[217] Reprinted (adapted) with permission from ref. 217. Copyright (2016) American Chemical Society.

5.4. Bio applications

Being the newest member of the carbon materials family, graphene possesses many unique physical properties resulting is a wide range of applications. Recently, it was discovered that GO can effectively adsorb DNA, and at the same time, it can completely quench adsorbed fluorophores. These properties make it possible to prepare DNA-based graphene materials for various bio applications in detection and cure of the diseases.

Wu *et al.*[218] described fluorescent-labeled oligonucleo-tides on GO surface. The binding between DNA and GO is strongly affected by both electrostatic repulsion and hydrophobic interactions. Cations, pH, and organic solvent can all be used to modulate DNA binding. Shorter DNA binds to the surface with faster kinetics and higher adsorption efficiency. Desorption can occur by adding the c-DNA to form ds-DNA, adding the same DNA to exchange, and increasing temperature. The temperature-induced desorption, however, was quite ineffective, suggesting a high binding affinity. Overall, the DNA binding to GO is very stable and reversible. These basic understandings of the surface interaction between DNA and GO are described in the Fig. 18. The mechanism of DNA adsorption and desorption on GO was explained by Park *et al.*[219]

Zhang *et al.*[220] demonstrated that uniform ultrasmall GO nanosheets has very low cytotoxicity and high cellular uptake. Therefore, the as-prepared uniform ultrasmall GO nanosheets

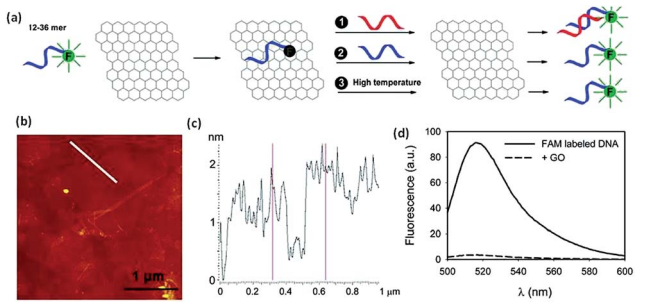

Fig. 18 (a) Schematic presentation of FAM-labeled DNA adsorption and desorption on GO. Fluorescence is quenched upon adsorption. Desorption can be achieved by adding the c-DNA (reaction 1), DNA exchange with the same DNA (reaction 2), or increasing temperature (reaction 3). (b) An AFM image showing GO sheets deposited on a silicon wafer. (c) The height profile of the line in (b) shows the sheets to be ~1.5 nm in thickness. (d) Fluorescence spectra of 100 nM 18-mer DNA in 25 mM HEPES, 100 mM NaCl, and 5 mM $MgCl_2$ in the presence and absence of 50 μg mL^{-1} of GO.[218] Reprinted (adapted) with permission from ref. 218. Copyright (2011) American Chemical Society.

could be explored as the ideal nanocarriers for drug delivery and intracellular fluorescent nanoprobe. Liu *et al.*[221] reported transferrin modified GO for glioma-targeted drug delivery and was evaluated *in vitro* and *in vivo* also. Zhang *et al.*[222] developed a GO-DTPA-Gd/DOX-based theranostic nanoplatform with dual modality T_1 MRI/fluorescence imaging and drug delivery functionalities. Weaver *et al.*[223] reported electrically controlled drug delivery nanocomposite composed of GO deposited inside a conducting polymer scaffold.

Various graphene based composites like (i) patterned substrates of nano-GO[224] (ii) GO/hydrogel-based angiogenic[225] (iii) hyaluronic acid-decorated GO nanohybrids[226] (iv) functionalized GO nanoparticles,[227] and (v) fluorescent GO *via* polymer grafting[227] *etc.* were utilized for efficient drug delivery. GO could be fabricated by modifying its functional groups to impart specific functional or structural attributes. This study demonstrated the development of a GO-based efficient gene delivery carrier through installation of polyethylenimine, a cationic polymer, which has been widely used as a non viral gene delivery vector. Kim *et al.*[228] demonstrated the successful fabrication of GO through covalent linkage with LMW BPEI, which acted as a cationic gene carrier. The BPEI-GO possessed high gene delivery efficiency and exhibited high cell viability. Furthermore, the PL properties of GO were enhanced through conjugation of BPEI to GO, which advocated the immense potential of BPEI-GO as a fluorescence reagent. Gold encapsulated nanoparticles or nanorods in GO shells showed a great response as a novel gene vector.[229]

Zhang *et al.*[230] grew porous platinum nanoparticles on GO which was proven to function as peroxidase mimetics that can catalyze the reaction of peroxidase substrate in the presence of hydrogen peroxide. On the basis of the peroxidase-like activity, this composite was utilized as a signal transducer to develop a colorimetric assay for the direct detection of cancer cells as described in the Fig. 19.

Fluorogenic resveratrol-confined GO were utilized for the detection of Alzheimer's disease by He *et al.*[231] MicroRNA in tumor cells were detected by using exonuclease III and GO-regulated signal amplification by Huang *et al.*[232] GO-capped mesoporous silica based drug could be released by remote control to cancer cells by photoinduced pH-jump activation as reported by He *et al.*[233]. Multifunctional hybrid nanopatches of GO and gold nanostars can be utilized for ultraefficient photothermal cancer therapy.[234] The photothermal therapeutic response of cancer cells to aptamer–gold nanoparticle-hybridized GO under NIR illumination was studied by Yang *et al.*[235] Multifunctional biocompatible GO quantum dots decorated magnetic nanoplatform were utilized for efficient capture and two-photon imaging of rare tumor cells.[235]

Demeritte *et al.*[236] reported hybrid GO based plasmonic-magnetic multifunctional nanoplatform for selective separation and label-free identification of Alzheimer's disease biomarkers biotin containing rGO based nano system was proved as a multi-effect anticancer agent by Mauro *et al.*[237] The hybrid based on rGO with ultrasmall gold nanorod were utilized for a sequential drug release and enhanced photothermal and photoacoustic effect for cancer therapy.[238] Zirconia/GO hybrid micromotors can selectively capture the nerve agents as reported by Singh *et al.*[239] Kenry *et al.*[240] investigated the cellular interactions between the breast cancer cells and the two-dimensional planar graphene material films. They observed the selective accelerated proliferation and increased cellular spreading areas coupled with minimal cytotoxicity of both malignant breast cancer cells induced by the planar GO film.

GO–silver nanocomposite were reported as a highly effective antibacterial agent with species-specific mechanisms.[241] This composite was also reported as a antibacterial against *Xanthomonas perforans* which causes a major disease of tomatoes, leading to reduction in production by 10–50%.[242] GO wrapped SERS tags can also be utilized as a multifunctional platforms toward optical labeling, photothermal ablation of bacteria, and the monitoring of killing effect.[243] Wang *et al.*[244] synthesized the ZnO/GO composites of varying contents of ZnO in high quality and these composites own superior antibacterial properties against *E. coli* with low cytotoxicity. Besides GO utilized as antibacterial agent as a killing dental pathogens.[245]

5.5. Biosensors applications

Sensors/biosensors allow an electronic device to become a gateway between the digital and physical worlds. Sensor materials with unprecedented performance can create new applications and new avenues for user interaction. Graphene and its related materials have attracted much interest in sensing applications because of their optimized ratio between active surface and bulk volume. In particular, several forms of oxidized graphene have been studied to optimize the sensing efficiency, sometimes moving away from practical solutions to boost performance.[246]

Biocompatible GO/functionalized GOs have been widely exploited for the sensing of biomolecules like (i) glucose,[247] (ii) amplified DNA,[248] (iii) D-glucosamine,[249] (iv) microRNA,[250] (v) DNA/RNA aptamers,[251] (vi) multiplexed microRNA,[252] (vii) optical aptamer,[253] (viii) arbitrary DNA mutations,[254] and (ix) luminescent iridium(III) complex labeled DNA.[255] GO based CuO nanoparticles composite electrode highly enhanced the nonenzymatic glucose detection.[256] A novel enzyme like activity of GO integrated with chitosan was demonstrated by Wang *et al.* and used as an efficient bio sensing system for glucose detection.[257]

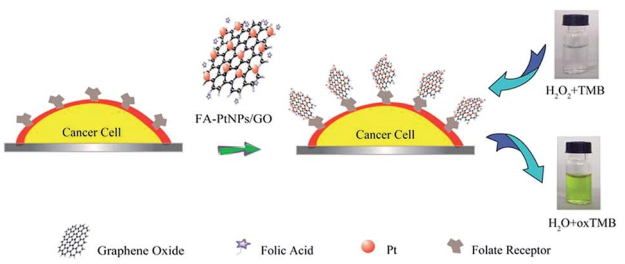

Fig. 19 Schematic representation of colorimetric direction of cancer cells by using folic acid functionalized PtNPs/GO.[230] Reprinted (adapted) with permission from ref. 230. Copyright (2011) American Chemical Society.

5.6. Sensors applications

Ren *et al.*[258] prepared GO/AgNP hybrids as SERS substrates for ultrasensitive and label-free SERS detection of folic acid in water and serum according to the inherent SERS spectra of folic acid. GO is also reported by various researchers as a ultrafast humidity sensors.[259–261] Paek *et al.*[262] developed a versatile platform for a highly stable, colorimetric, wide-range pH sensor. This pH sensor consisted of responsive polymer and QD hybrids integrated onto the surface of GO. The distances between the two color-emitting QDs and the GO were controlled independently *via* two linkers of pH-responsive poly(acrylic acid) (PAA) and poly(2-vinylpyridine) (P2VP), resulting in colorimetric responses over a wide range of pH values. Pt-decorated GO nanostructures were utilized by Wang *et al.* as a hydrogen gas sensor.[263]

6. Conclusions and outlook

In this review we have intended to address the continued developments and challenges with a wide scope of interest, highlighting fundamental understanding of the synthesis, characterization, reduction of GO and its potential applications in various research fields. Graphene oxide and reduced graphene oxide (incomplete reduction into graphene due to the limited capacity of reducing agents), because of various containing functional groups like epoxy, hydroxyl, carboxyl and carbonyl, and various defects/disordered caused during reduction provide an efficient tool and a broad scope to scientific community for its widespread applications in emerging research areas of interest like energy sector and biomedicine. The GO is also a useful platform for the fabrication of functionalized graphene that can potentially confer improved mechanical, thermal and electronic properties *etc.* Readily available functional groups set up to bind with various other nanostructures, drugs and biological molecules like DNA, peptide, aptamer, protein, lipids *etc.* make graphene oxide as one of the most suitable candidate for energy storage, electrochemical devices, biosensors, catalysis, imaging/mapping of the cancer cells, photo-thermal therapy, targeted drug delivery, contamination purification and extraction devices for chemical, biological, and environmental samples. Various simple, large scale and cost effective methods discussed in the review have not only opened its application in the areas where we require large amount of materials but with reduced cost specially for drug design and delivery, the treatment/cure of life-threatening diseases like cancer and AIDS. Huge number of published research and works being done have not only proved its supremacy over other nanomaterials used so far but also continuously surprising researcher's mind with its new hope and possibilities day by day.

Acknowledgements

Author D. P. Singh acknowledges with gratitude the financial support from CONICYT Chile (FONDECYT REGULAR 1151527).

Notes and references

1 J. Pedrós, A. Boscá, J. Martínez, S. Ruiz-Gómez, L. Pérez, V. Barranco and F. Calle, *J. Power Sources*, 2016, **317**, 35–42.
2 M. S. Dresselhaus, A. Jorio and R. Saito, *Annu. Rev. Condens. Matter Phys.*, 2010, **1**, 89–108.
3 A. K. Geim and K. S. Novoselov, *Nat. Mater.*, 2007, **6**, 183–191.
4 E. C. H. Sykes, *Nat. Chem.*, 2009, **1**, 175–176.
5 D. Li and R. B. Kaner, *Science*, 2008, **320**, 1170–1171.
6 V. Singh, D. Joung, L. Zhai, S. Das, S. I. Khondaker and S. Seal, *Prog. Mater. Sci.*, 2011, **56**, 1178–1271.
7 S. V. Morozov, K. S. Novoselov, M. I. Katsnelson, F. Schedin, D. C. Elias, J. A. Jaszczak and A. K. Geim, *Phys. Rev. Lett.*, 2008, **100**, 016602.
8 K. I. Bolotin, K. J. Sikes, Z. Jiang, M. Klima, G. Fudenberg, J. Hone, P. Kim and H. L. Stormer, *Solid State Commun.*, 2008, **146**, 351–355.
9 A. A. Balandin, S. Ghosh, W. Bao, I. Calizo, D. Teweldebrhan, F. Miao and C. N. Lau, *Nano Lett.*, 2008, **8**, 902–907.
10 F. Bonaccorso, L. Colombo, G. Yu, M. Stoller, V. Tozzini, A. C. Ferrari, R. S. Ruoff and V. Pellegrini, *Science*, 2015, **347**, 6217.
11 C. Lee, X. Wei, J. W. Kysar and J. Hone, *Science*, 2008, **321**, 385–388.
12 F. Bonaccorso, Z. Sun, T. Hasan and A. C. Ferrari, *Nat. Photonics*, 2010, **4**, 611–622.
13 B. Marinho, M. Ghislandi, E. Tkalya, C. E. Koning and G. de With, *Powder Technol.*, 2012, **221**, 351–358.
14 A. J. Van Bommel, J. E. Crombeen and A. Van Tooren, *Surf. Sci.*, 1975, **48**, 463–472.
15 H. P. Boehm, R. Setton and E. Stumpp, *Carbon*, 1986, **24**, 241–245.
16 X. Lu, H. Huang, N. Nemchuk and R. S. Ruoff, *Appl. Phys. Lett.*, 1999, **75**, 193–195.
17 J. Wintterlin and M. L. Bocquet, *Surf. Sci.*, 2009, **603**, 1841–1852.
18 L. Xuekun, Y. Minfeng, H. Hui and S. R. Rodney, *Nanotechnology*, 1999, **10**, 269.
19 H. P. Boehm, A. Clauss, G. O. Fischer and U. Hofmann, *Z. Anorg. Allg. Chem.*, 1962, **316**, 119–127.
20 K. S. Novoselov, A. K. Geim, S. V. Morozov, D. Jiang, Y. Zhang, S. V. Dubonos, I. V. Grigorieva and A. A. Firsov, *Science*, 2004, **306**, 666–669.
21 C. Berger, Z. Song, T. Li, X. Li, A. Y. Ogbazghi, R. Feng, Z. Dai, A. N. Marchenkov, E. H. Conrad, P. N. First and W. A. de Heer, *J. Phys. Chem. B*, 2004, **108**, 19912–19916.
22 X. Li, W. Cai, J. An, S. Kim, J. Nah, D. Yang, R. Piner, A. Velamakanni, I. Jung, E. Tutuc, S. K. Banerjee, L. Colombo and R. S. Ruoff, *Science*, 2009, **324**, 1312–1314.
23 C. Berger, Z. Song, X. Li, X. Wu, N. Brown, C. Naud, D. Mayou, T. Li, J. Hass, A. N. Marchenkov, E. H. Conrad, P. N. First and W. A. de Heer, *Science*, 2006, **312**, 1191–1196.
24 T. A. Land, T. Michely, R. J. Behm, J. C. Hemminger and G. Comsa, *Surf. Sci.*, 1992, **264**, 261–270.

25 K. S. Kim, Y. Zhao, H. Jang, S. Y. Lee, J. M. Kim, K. S. Kim, J. H. Ahn, P. Kim, J. Y. Choi and B. H. Hong, *Nature*, 2009, **457**, 706–710.
26 M. Eizenberg and J. M. Blakely, *Surf. Sci.*, 1979, **82**, 228–236.
27 B. C. Brodie, *Philos. Trans. R. Soc. London*, 1859, **149**, 249–259.
28 W. S. Hummers and R. E. Offeman, *J. Am. Chem. Soc.*, 1958, **80**, 1339.
29 L. Staudenmaier, *Ber. Dtsch. Chem. Ges.*, 1898, **31**, 1481–1487.
30 U. Hofmann and E. König, *Z. Anorg. Allg. Chem.*, 1937, **234**, 311–336.
31 Z. Liu, S. P. Lau and F. Yan, *Chem. Soc. Rev.*, 2015, **44**, 5638–5679.
32 F. Perreault, A. Fonseca de Faria and M. Elimelech, *Chem. Soc. Rev.*, 2015, **44**, 5861–5896.
33 K. Chen, S. Song, F. Liu and D. Xue, *Chem. Soc. Rev.*, 2015, **44**, 6230–6257.
34 S. Guo and S. Dong, *Chem. Soc. Rev.*, 2011, **40**, 2644–2672.
35 Y. Liu, X. Dong and P. Chen, *Chem. Soc. Rev.*, 2012, **41**, 2283–2307.
36 D. R. Dreyer, S. Park, C. W. Bielawski and R. S. Ruoff, *Chem. Soc. Rev.*, 2010, **39**, 228–240.
37 W. Gao, L. B. Alemany, L. Ci and P. M. Ajayan, *Nat. Chem.*, 2009, **1**, 403–408.
38 A. Lerf, H. He, M. Forster and J. Klinowski, *J. Phys. Chem. B*, 1998, **102**, 4477–4482.
39 T. Szabó, O. Berkesi, P. Forgó, K. Josepovits, Y. Sanakis, D. Petridis and I. Dékány, *Chem. Mater.*, 2006, **18**, 2740–2749.
40 R. Ruoff, *Nat. Nanotechnol.*, 2008, **3**, 10–11.
41 K. A. Mkhoyan, A. W. Contryman, J. Silcox, D. A. Stewart, G. Eda, C. Mattevi, S. Miller and M. Chhowalla, *Nano Lett.*, 2009, **9**, 1058–1063.
42 F. Kim, L. J. Cote and J. Huang, *Adv. Mater.*, 2010, **22**, 1954–1958.
43 G. Eda and M. Chhowalla, *Adv. Mater.*, 2010, **22**, 2392–2415.
44 X. Li, G. Zhang, X. Bai, X. Sun, X. Wang, E. Wang and H. Dai, *Nat. Nanotechnol.*, 2008, **3**, 538–542.
45 Y. Obeng and P. Srinivasan, *Electrochem. Soc. Interface*, 2011, **20**, 47–52.
46 C. Schafhaeutl, *J. Prakt. Chem.*, 1840, **21**, 129–157.
47 C. Schafhaeutl, *Philos. Mag.*, 1840, **16**, 570–590.
48 U. Hofmann and R. Holst, *Ber. Dtsch. Chem. Ges.*, 1939, **72**, 754–771.
49 C. Botas, P. Álvarez, P. Blanco, M. Granda, C. Blanco, R. Santamaría, L. J. Romasanta, R. Verdejo, M. A. López-Manchado and R. Menéndez, *Carbon*, 2013, **65**, 156–164.
50 A. C. Ferrari, F. Bonaccorso, V. Fal'ko, K. S. Novoselov, S. Roche, P. Boggild, S. Borini, F. H. L. Koppens, V. Palermo, N. Pugno, J. A. Garrido, R. Sordan, A. Bianco, L. Ballerini, M. Prato, E. Lidorikis, J. Kivioja, C. Marinelli, T. Ryhanen, A. Morpurgo, J. N. Coleman, V. Nicolosi, L. Colombo, A. Fert, M. Garcia-Hernandez, A. Bachtold, G. F. Schneider, F. Guinea, C. Dekker, M. Barbone, Z. Sun, C. Galiotis, A. N. Grigorenko, G. Konstantatos, A. Kis, M. Katsnelson, L. Vandersypen, A. Loiseau, V. Morandi, D. Neumaier, E. Treossi, V. Pellegrini, M. Polini, A. Tredicucci, G. M. Williams, B. Hee Hong, J.-H. Ahn, J. Min Kim, H. Zirath, B. J. van Wees, H. van der Zant, L. Occhipinti, A. Di Matteo, I. A. Kinloch, T. Seyller, E. Quesnel, X. Feng, K. Teo, N. Rupesinghe, P. Hakonen, S. R. T. Neil, Q. Tannock, T. Lofwander and J. Kinaret, *Nanoscale*, 2015, **7**, 4598–4810.
51 Q.-L. Yan, M. Gozin, F.-Q. Zhao, A. Cohen and S.-P. Pang, *Nanoscale*, 2016, **8**, 4799–4851.
52 T. Kuila, A. K. Mishra, P. Khanra, N. H. Kim and J. H. Lee, *Nanoscale*, 2013, **5**, 52–71.
53 S. Mao, H. Pu and J. Chen, *RSC Adv.*, 2012, **2**, 2643–2662.
54 H.-K. Jeong, Y. P. Lee, R. J. W. E. Lahaye, M.-H. Park, K. H. An, I. J. Kim, C.-W. Yang, C. Y. Park, R. S. Ruoff and Y. H. Lee, *J. Am. Chem. Soc.*, 2008, **130**, 1362–1366.
55 R. Kumar, H.-J. Kim, S. Park, A. Srivastava and I.-K. Oh, *Carbon*, 2014, **79**, 192–202.
56 R. Sun, H.-B. Zhang, J. Yao, D. Yang, Y.-W. Mai and Z.-Z. Yu, *Carbon*, DOI: 10.1016/j.carbon.2016.05.041.
57 H. L. Poh, F. Šaněk, A. Ambrosi, G. Zhao, Z. Sofer and M. Pumera, *Nanoscale*, 2012, **4**, 3515–3522.
58 C. Hontoria-Lucas, A. J. López-Peinado, J. d. D. López-González, M. L. Rojas-Cervantes and R. M. Martín-Aranda, *Carbon*, 1995, **33**, 1585–1592.
59 Y.-Y. Peng, Y.-M. Liu, J.-K. Chang, C.-H. Wu, M.-D. Ger, N.-W. Pu and C.-L. Chang, *Carbon*, 2015, **81**, 347–356.
60 C. H. A. Wong, O. Jankovský, Z. Sofer and M. Pumera, *Carbon*, 2014, **77**, 508–517.
61 H. L. Poh, P. Šimek, Z. Sofer and M. Pumera, *ACS Nano*, 2013, **7**, 5262–5272.
62 D. Sačer, D. Čapeta, I. Šrut Rakić, R. Peter, M. Petravić and M. Kraljić Roković, *Electrochim. Acta*, 2016, **193**, 311–320.
63 G. Zhao, J. Li, X. Ren, C. Chen and X. Wang, *Environ. Sci. Technol.*, 2011, **45**, 10454–10462.
64 D. C. Marcano, D. V. Kosynkin, J. M. Berlin, A. Sinitskii, Z. Sun, A. Slesarev, L. B. Alemany, W. Lu and J. M. Tour, *ACS Nano*, 2010, **4**, 4806–4814.
65 J. Chen, B. Yao, C. Li and G. Shi, *Carbon*, 2013, **64**, 225–229.
66 J. Chen, Y. Li, L. Huang, C. Li and G. Shi, *Carbon*, 2015, **81**, 826–834.
67 J. Guerrero-Contreras and F. Caballero-Briones, *Mater. Chem. Phys.*, 2015, **153**, 209–220.
68 C.-I. Chang, K.-H. Chang, H.-H. Shen and C.-C. Hu, *J. Taiwan Inst. Chem. Eng.*, 2014, **45**, 2762–2769.
69 J. H. Kang, T. Kim, J. Choi, J. Park, Y. S. Kim, M. S. Chang, H. Jung, K. T. Park, S. J. Yang and C. R. Park, *Chem. Mater.*, 2016, **28**, 756–764.
70 U. Saha, R. Jaiswal and T. H. Goswami, *Electrochim. Acta*, 2016, **196**, 386–404.
71 D. Pacilé, J. C. Meyer, A. Fraile Rodríguez, M. Papagno, C. Gómez-Navarro, R. S. Sundaram, M. Burghard, K. Kern, C. Carbone and U. Kaiser, *Carbon*, 2011, **49**, 966–972.
72 J. Shen, Y. Hu, M. Shi, X. Lu, C. Qin, C. Li and M. Ye, *Chem. Mater.*, 2009, **21**, 3514–3520.
73 M. Wissler, *J. Power Sources*, 2006, **156**, 142–150.
74 A. Dimiev, D. V. Kosynkin, L. B. Alemany, P. Chaguine and J. M. Tour, *J. Am. Chem. Soc.*, 2012, **134**, 2815–2822.

75 C. Mattevi, G. Eda, S. Agnoli, S. Miller, K. A. Mkhoyan, O. Celik, D. Mastrogiovanni, G. Granozzi, E. Garfunkel and M. Chhowalla, *Adv. Funct. Mater.*, 2009, **19**, 2577–2583.
76 A. Ganguly, S. Sharma, P. Papakonstantinou and J. Hamilton, *J. Phys. Chem. C*, 2011, **115**, 17009–17019.
77 W. Zhang, V. Carravetta, Z. Li, Y. Luo and J. Yang, *J. Chem. Phys.*, 2009, **131**, 244505.
78 D. W. Lee, L. V. De Los Santos, J. W. Seo, L. L. Felix, A. Bustamante, D. J. M. Cole and C. H. W. Barnes, *J. Phys. Chem. B*, 2010, **114**, 5723–5728.
79 J. I. Paredes, S. Villar-Rodil, P. Solís-Fernández, A. Martínez-Alonso and J. M. D. Tascón, *Langmuir*, 2009, **25**, 5957–5968.
80 S. Saxena, T. A. Tyson and E. Negusse, *J. Phys. Chem. Lett.*, 2010, **1**, 3433–3437.
81 V. Lee, L. Whittaker, C. Jaye, K. M. Baroudi, D. A. Fischer and S. Banerjee, *Chem. Mater.*, 2009, **21**, 3905–3916.
82 A. Bagri, C. Mattevi, M. Acik, Y. J. Chabal, M. Chhowalla and V. B. Shenoy, *Nat. Chem.*, 2010, **2**, 581–587.
83 M. Acik, G. Lee, C. Mattevi, A. Pirkle, R. M. Wallace, M. Chhowalla, K. Cho and Y. Chabal, *J. Phys. Chem. C*, 2011, **115**, 19761–19781.
84 Y. Si and E. T. Samulski, *Nano Lett.*, 2008, **8**, 1679–1682.
85 K. N. Kudin, B. Ozbas, H. C. Schniepp, R. K. Prud'homme, I. A. Aksay and R. Car, *Nano Lett.*, 2008, **8**, 36–41.
86 W. Cai, R. D. Piner, F. J. Stadermann, S. Park, M. A. Shaibat, Y. Ishii, D. Yang, A. Velamakanni, S. J. An, M. Stoller, J. An, D. Chen and R. S. Ruoff, *Science*, 2008, **321**, 1815–1817.
87 L. B. Casabianca, M. A. Shaibat, W. W. Cai, S. Park, R. Piner, R. S. Ruoff and Y. Ishii, *J. Am. Chem. Soc.*, 2010, **132**, 5672–5676.
88 D. Yang, A. Velamakanni, G. Bozoklu, S. Park, M. Stoller, R. D. Piner, S. Stankovich, I. Jung, D. A. Field, C. A. Ventrice Jr and R. S. Ruoff, *Carbon*, 2009, **47**, 145–152.
89 O. Akhavan, *Carbon*, 2010, **48**, 509–519.
90 H. C. Schniepp, J.-L. Li, M. J. McAllister, H. Sai, M. Herrera-Alonso, D. H. Adamson, R. K. Prud'homme, R. Car, D. A. Saville and I. A. Aksay, *J. Phys. Chem. B*, 2006, **110**, 8535–8539.
91 B. Sun, X. Huang, S. Chen, P. Munroe and G. Wang, *Nano Lett.*, 2014, **14**, 3145–3152.
92 M. A. Pimenta, G. Dresselhaus, M. S. Dresselhaus, L. G. Cancado, A. Jorio and R. Saito, *Phys. Chem. Chem. Phys.*, 2007, **9**, 1276–1290.
93 C. K. Chua and M. Pumera, *Chem. Soc. Rev.*, 2014, **43**, 291–312.
94 S. Pei and H.-M. Cheng, *Carbon*, 2012, **50**, 3210–3228.
95 S. Stankovich, D. A. Dikin, R. D. Piner, K. A. Kohlhaas, A. Kleinhammes, Y. Jia, Y. Wu, S. T. Nguyen and R. S. Ruoff, *Carbon*, 2007, **45**, 1558–1565.
96 H. Bai, C. Li and G. Shi, *Adv. Mater.*, 2011, **23**, 1089–1115.
97 H.-J. Shin, K. K. Kim, A. Benayad, S.-M. Yoon, H. K. Park, I.-S. Jung, M. H. Jin, H.-K. Jeong, J. M. Kim, J.-Y. Choi and Y. H. Lee, *Adv. Funct. Mater.*, 2009, **19**, 1987–1992.
98 X. Fan, W. Peng, Y. Li, X. Li, S. Wang, G. Zhang and F. Zhang, *Adv. Mater.*, 2008, **20**, 4490–4493.
99 V. H. Pham, T. V. Cuong, T.-D. Nguyen-Phan, H. D. Pham, E. J. Kim, S. H. Hur, E. W. Shin, S. Kim and J. S. Chung, *Chem. Commun.*, 2010, **46**, 4375–4377.
100 T. Cassagneau and J. H. Fendler, *J. Phys. Chem. B*, 1999, **103**, 1789–1793.
101 J. Zhang, H. Yang, G. Shen, P. Cheng, J. Zhang and S. Guo, *Chem. Commun.*, 2010, **46**, 1112–1114.
102 M. J. Fernández-Merino, L. Guardia, J. I. Paredes, S. Villar-Rodil, P. Solís-Fernández, A. Martínez-Alonso and J. M. D. Tascón, *J. Phys. Chem. C*, 2010, **114**, 6426–6432.
103 Z. Li, Y. Yao, Z. Lin, K.-S. Moon, W. Lin and C. Wong, *J. Mater. Chem.*, 2010, **20**, 4781–4783.
104 X. Zhou, J. Zhang, H. Wu, H. Yang, J. Zhang and S. Guo, *J. Phys. Chem. C*, 2011, **115**, 11957–11961.
105 G. Wang, J. Yang, J. Park, X. Gou, B. Wang, H. Liu and J. Yao, *J. Phys. Chem. C*, 2008, **112**, 8192–8195.
106 C. A. Amarnath, C. E. Hong, N. H. Kim, B.-C. Ku, T. Kuila and J. H. Lee, *Carbon*, 2011, **49**, 3497–3502.
107 J. Gao, F. Liu, Y. Liu, N. Ma, Z. Wang and X. Zhang, *Chem. Mater.*, 2010, **22**, 2213–2218.
108 T. A. Pham, J. S. Kim, J. S. Kim and Y. T. Jeong, *Colloids Surf., A*, 2011, **384**, 543–548.
109 Z. Lei, L. Lu and X. S. Zhao, *Energy Environ. Sci.*, 2012, **5**, 6391–6399.
110 H. A. Becerril, J. Mao, Z. Liu, R. M. Stoltenberg, Z. Bao and Y. Chen, *ACS Nano*, 2008, **2**, 463–470.
111 X. Wang, L. Zhi and K. Müllen, *Nano Lett.*, 2008, **8**, 323–327.
112 X. Li, H. Wang, J. T. Robinson, H. Sanchez, G. Diankov and H. Dai, *J. Am. Chem. Soc.*, 2009, **131**, 15939–15944.
113 Z.-S. Wu, W. Ren, L. Gao, J. Zhao, Z. Chen, B. Liu, D. Tang, B. Yu, C. Jiang and H.-M. Cheng, *ACS Nano*, 2009, **3**, 411–417.
114 G. I. Titelman, V. Gelman, S. Bron, R. L. Khalfin, Y. Cohen and H. Bianco-Peled, *Carbon*, 2005, **43**, 641–649.
115 M. J. McAllister, J.-L. Li, D. H. Adamson, H. C. Schniepp, A. A. Abdala, J. Liu, M. Herrera-Alonso, D. L. Milius, R. Car, R. K. Prud'homme and I. A. Aksay, *Chem. Mater.*, 2007, **19**, 4396–4404.
116 A. M. Schwenke, S. Hoeppener and U. S. Schubert, *J. Mater. Chem. A*, 2015, **3**, 23778–23787.
117 Y. Zhu, S. Murali, M. D. Stoller, A. Velamakanni, R. D. Piner and R. S. Ruoff, *Carbon*, 2010, **48**, 2118–2122.
118 H. M. A. Hassan, V. Abdelsayed, A. E. R. S. Khder, K. M. AbouZeid, J. Terner, M. S. El-Shall, S. I. Al-Resayes and A. A. El-Azhary, *J. Mater. Chem.*, 2009, **19**, 3832–3837.
119 Y. Zhang, L. Guo, S. Wei, Y. He, H. Xia, Q. Chen, H.-B. Sun and F.-S. Xiao, *Nano Today*, 2010, **5**, 15–20.
120 L. J. Cote, R. Cruz-Silva and J. Huang, *J. Am. Chem. Soc.*, 2009, **131**, 11027–11032.
121 T. V. Khai, D. S. Kwak, Y. J. Kwon, H. Y. Cho, T. N. Huan, H. Chung, H. Ham, C. Lee, N. V. Dan, N. T. Tung and H. W. Kim, *Chem. Eng. J.*, 2013, **232**, 346–355.
122 H. J. Han, Y. N. Chen and Z. J. Wang, *RSC Adv.*, 2015, **5**, 92940–92946.
123 T. Lu, L. Pan, C. Nie, Z. Zhao and Z. Sun, *Phys. Status Solidi A*, 2011, **208**, 2325–2327.
124 D. Sun, L. Jin, Y. Chen, J.-R. Zhang and J.-J. Zhu, *ChemPlusChem*, 2013, **78**, 227–234.
125 A. Y. S. Eng, Z. Sofer, P. Šimek, J. Kosina and M. Pumera, *Chem.–Eur. J.*, 2013, **19**, 15583–15592.

126 A. M. Schwenke, S. Hoeppener and U. S. Schubert, *Adv. Mater.*, 2015, **27**, 4113–4141.
127 Q. Yan, Q. Liu and J. Wang, *Ceram. Int.*, 2016, **42**, 3007–3013.
128 W. Chen, L. Yan and P. R. Bangal, *Carbon*, 2010, **48**, 1146–1152.
129 C. N. R. Rao, K. S. Subrahmanyam, H. S. S. R. Matte, B. Abdulhakeem, A. Govindaraj, D. Barun, K. Prashant, G. Anupama and J. L. Dattatray, *Sci. Technol. Adv. Mater.*, 2010, **11**, 054502.
130 Y. H. Ding, P. Zhang, Q. Zhuo, H. M. Ren, Z. M. Yang and Y. Jiang, *Nanotechnology*, 2011, **22**, 215601.
131 V. Abdelsayed, S. Moussa, H. M. Hassan, H. S. Aluri, M. M. Collinson and M. S. El-Shall, *J. Phys. Chem. Lett.*, 2010, **1**, 2804–2809.
132 P. Kumar, B. Das, B. Chitara, K. S. Subrahmanyam, K. Gopalakrishnan, S. B. Krupanidhi and C. N. R. Rao, *Macromol. Chem. Phys.*, 2012, **213**, 1146–1163.
133 P. Kumar, K. S. Subrahmanyam and C. N. R. Rao, *Mater. Express*, 2011, **1**, 252–256.
134 M. Baraket, S. G. Walton, Z. Wei, E. H. Lock, J. T. Robinson and P. Sheehan, *Carbon*, 2010, **48**, 3382–3390.
135 O. Ö. Ekiz, M. Ürel, H. Güner, A. K. Mizrak and A. Dâna, *ACS Nano*, 2011, **5**, 2475–2482.
136 P. Yao, P. Chen, L. Jiang, H. Zhao, H. Zhu, D. Zhou, W. Hu, B.-H. Han and M. Liu, *Adv. Mater.*, 2010, **22**, 5008–5012.
137 G. Williams, B. Seger and P. V. Kamat, *ACS Nano*, 2008, **2**, 1487–1491.
138 P. V. Kamat, *Chem. Rev.*, 1993, **93**, 267–300.
139 H. Zhang, X. Lv, Y. Li, Y. Wang and J. Li, *ACS Nano*, 2010, **4**, 380–386.
140 S. R. Kim, M. K. Parvez and M. Chhowalla, *Chem. Phys. Lett.*, 2009, **483**, 124–127.
141 N. Yang, J. Zhai, D. Wang, Y. Chen and L. Jiang, *ACS Nano*, 2010, **4**, 887–894.
142 A. Kongkanand and P. V. Kamat, *ACS Nano*, 2007, **1**, 13–21.
143 P. V. Kamat, I. Bedja and S. Hotchandani, *J. Phys. Chem.*, 1994, **98**, 9137–9142.
144 G. Williams and P. V. Kamat, *Langmuir*, 2009, **25**, 13869–13873.
145 S. Dubin, S. Gilje, K. Wang, V. C. Tung, K. Cha, A. S. Hall, J. Farrar, R. Varshneya, Y. Yang and R. B. Kaner, *ACS Nano*, 2010, **4**, 3845–3852.
146 H. Wang, J. T. Robinson, X. Li and H. Dai, *J. Am. Chem. Soc.*, 2009, **131**, 9910–9911.
147 Y. Zhou, Q. Bao, L. A. L. Tang, Y. Zhong and K. P. Loh, *Chem. Mater.*, 2009, **21**, 2950–2956.
148 G. Demazeau, *J. Mater. Chem.*, 1999, **9**, 15–18.
149 X. Sun and Y. Li, *Angew. Chem., Int. Ed.*, 2004, **43**, 597–601.
150 L.-B. Luo, S.-H. Yu, H.-S. Qian and T. Zhou, *J. Am. Chem. Soc.*, 2005, **127**, 2822–2823.
151 D. Li, M. B. Muller, S. Gilje, R. B. Kaner and G. G. Wallace, *Nat. Nanotechnol.*, 2008, **3**, 101–105.
152 X. Shen, L. Jiang, Z. Ji, J. Wu, H. Zhou and G. Zhu, *J. Colloid Interface Sci.*, 2011, **354**, 493–497.
153 W. Chen, L. Yan and P. R. Bangal, *J. Phys. Chem. C*, 2010, **114**, 19885–19890.
154 C. Zhu, S. Guo, Y. Fang and S. Dong, *ACS Nano*, 2010, **4**, 2429–2437.
155 Z.-J. Fan, W. Kai, J. Yan, T. Wei, L.-J. Zhi, J. Feng, Y.-M. Ren, L.-P. Song and F. Wei, *ACS Nano*, 2011, **5**, 191–198.
156 R. S. Dey, S. Hajra, R. K. Sahu, C. R. Raj and M. K. Panigrahi, *Chem. Commun.*, 2012, **48**, 1787–1789.
157 T. S. Sreeprasad, A. K. Samal and T. Pradeep, *J. Phys. Chem. C*, 2009, **113**, 1727–1737.
158 C. Nethravathi and M. Rajamathi, *Carbon*, 2008, **46**, 1994–1998.
159 W. Chen and L. Yan, *Nanoscale*, 2010, **2**, 559–563.
160 X. Zhu, Y. Zhu, S. Murali, M. D. Stoller and R. S. Ruoff, *ACS Nano*, 2011, **5**, 3333–3338.
161 F. Zhang, H. Cao, D. Yue, J. Zhang and M. Qu, *Inorg. Chem.*, 2012, **51**, 9544–9551.
162 B. Wang, X. Li, X. Zhang, B. Luo, M. Jin, M. Liang, S. A. Dayeh, S. T. Picraux and L. Zhi, *ACS Nano*, 2013, **7**, 1437–1445.
163 A. Bhaskar, M. Deepa, M. Ramakrishna and T. N. Rao, *J. Phys. Chem. C*, 2014, **118**, 7296–7306.
164 X. Guan, J. Nai, Y. Zhang, P. Wang, J. Yang, L. Zheng, J. Zhang and L. Guo, *Chem. Mater.*, 2014, **26**, 5958–5964.
165 J. Yao, Y. Gong, S. Yang, P. Xiao, Y. Zhang, K. Keyshar, G. Ye, S. Ozden, R. Vajtai and P. M. Ajayan, *ACS Appl. Mater. Interfaces*, 2014, **6**, 20414–20422.
166 Y. Xu, X. Zhu, X. Zhou, X. Liu, Y. Liu, Z. Dai and J. Bao, *J. Phys. Chem. C*, 2014, **118**, 28502–28508.
167 C. Zhang, N. Mahmood, H. Yin, F. Liu and Y. Hou, *Adv. Mater.*, 2013, **25**, 4932–4937.
168 D. Yoon, K. Y. Chung, W. Chang, S. M. Kim, M. J. Lee, Z. Lee and J. Kim, *Chem. Mater.*, 2015, **27**, 266–275.
169 X. Liu, J. Zhang, W. Si, L. Xi, B. Eichler, C. Yan and O. G. Schmidt, *ACS Nano*, 2015, **9**, 1198–1205.
170 G. Zeng, N. Shi, M. Hess, X. Chen, W. Cheng, T. Fan and M. Niederberger, *ACS Nano*, 2015, **9**, 4227–4235.
171 X. Gao, J. Li, Y. Xie, D. Guan and C. Yuan, *ACS Appl. Mater. Interfaces*, 2015, **7**, 7855–7862.
172 F. Xiong, Z. Cai, L. Qu, P. Zhang, Z. Yuan, O. K. Asare, W. Xu, C. Lin and L. Mai, *ACS Appl. Mater. Interfaces*, 2015, **7**, 12625–12630.
173 S. H. Choi, K. Y. Jung and Y. C. Kang, *ACS Appl. Mater. Interfaces*, 2015, **7**, 13952–13959.
174 C. Feng, L. Zhang, M. Yang, X. Song, H. Zhao, Z. Jia, K. Sun and G. Liu, *ACS Appl. Mater. Interfaces*, 2015, **7**, 15726–15734.
175 A. R. Park, D.-Y. Son, J. S. Kim, J. Y. Lee, N.-G. Park, J. Park, J. K. Lee and P. J. Yoo, *ACS Appl. Mater. Interfaces*, 2015, **7**, 18483–18490.
176 X. Xu, S. Ji, M. Gu and J. Liu, *ACS Appl. Mater. Interfaces*, 2015, **7**, 20957–20964.
177 X. Wei, C. Tang, X. Wang, L. Zhou, Q. Wei, M. Yan, J. Sheng, P. Hu, B. Wang and L. Mai, *ACS Appl. Mater. Interfaces*, 2015, **7**, 26572–26578.
178 H. Xu, L. Shi, Z. Wang, J. Liu, J. Zhu, Y. Zhao, M. Zhang and S. Yuan, *ACS Appl. Mater. Interfaces*, 2015, **7**, 27486–27493.
179 K. S. Lee, S. Park, W. Lee and Y. S. Yoon, *ACS Appl. Mater. Interfaces*, 2016, **8**, 2027–2034.

180 Y. Luo, X. Xu, Y. Zhang, C.-Y. Chen, L. Zhou, M. Yan, Q. Wei, X. Tian and L. Mai, *ACS Appl. Mater. Interfaces*, 2016, **8**, 2812–2818.
181 S. H. Ha, Y. S. Jeong and Y. J. Lee, *ACS Appl. Mater. Interfaces*, 2013, **5**, 12295–12303.
182 Z. Guo, D. Zhang, H. Qiu, T. Zhang, Q. Fu, L. Zhang, X. Yan, X. Meng, G. Chen and Y. Wei, *ACS Appl. Mater. Interfaces*, 2015, **7**, 13972–13979.
183 L. Ji, M. Rao, H. Zheng, L. Zhang, Y. Li, W. Duan, J. Guo, E. J. Cairns and Y. Zhang, *J. Am. Chem. Soc.*, 2011, **133**, 18522–18525.
184 W. Zhou, H. Chen, Y. Yu, D. Wang, Z. Cui, F. J. DiSalvo and H. D. Abruña, *ACS Nano*, 2013, **7**, 8801–8808.
185 J. Rong, M. Ge, X. Fang and C. Zhou, *Nano Lett.*, 2014, **14**, 473–479.
186 C. Wang, X. Wang, Y. Yang, A. Kushima, J. Chen, Y. Huang and J. Li, *Nano Lett.*, 2015, **15**, 1796–1802.
187 Y. Hwa, J. Zhao and E. J. Cairns, *Nano Lett.*, 2015, **15**, 3479–3486.
188 J.-Q. Huang, T.-Z. Zhuang, Q. Zhang, H.-J. Peng, C.-M. Chen and F. Wei, *ACS Nano*, 2015, **9**, 3002–3011.
189 H.-G. Jung, Y. S. Jeong, J.-B. Park, Y.-K. Sun, B. Scrosati and Y. J. Lee, *ACS Nano*, 2013, **7**, 3532–3539.
190 R. Black, J.-H. Lee, B. Adams, C. A. Mims and L. F. Nazar, *Angew. Chem.*, 2013, **125**, 410–414.
191 Y. Li, J. Wang, X. Li, D. Geng, R. Li and X. Sun, *Chem. Commun.*, 2011, **47**, 9438–9440.
192 Y. Li, J. Wang, X. Li, D. Geng, M. N. Banis, Y. Tang, D. Wang, R. Li, T.-K. Sham and X. Sun, *J. Mater. Chem.*, 2012, **22**, 20170–20174.
193 Y. Li, J. Wang, X. Li, D. Geng, M. N. Banis, R. Li and X. Sun, *Electrochem. Commun.*, 2012, **18**, 12–15.
194 S.-S. Li, K.-H. Tu, C.-C. Lin, C.-W. Chen and M. Chhowalla, *ACS Nano*, 2010, **4**, 3169–3174.
195 J. Liu, Y. Xue and L. Dai, *J. Phys. Chem. Lett.*, 2012, **3**, 1928–1933.
196 J. G. Radich, R. Dwyer and P. V. Kamat, *J. Phys. Chem. Lett.*, 2011, **2**, 2453–2460.
197 I. P. Murray, S. J. Lou, L. J. Cote, S. Loser, C. J. Kadleck, T. Xu, J. M. Szarko, B. S. Rolczynski, J. E. Johns, J. Huang, L. Yu, L. X. Chen, T. J. Marks and M. C. Hersam, *J. Phys. Chem. Lett.*, 2011, **2**, 3006–3012.
198 L. Kavan, J.-H. Yum and M. Graetzel, *ACS Appl. Mater. Interfaces*, 2012, **4**, 6999–7006.
199 Y. Li, H. Wang, Q. Feng, G. Zhou and Z.-S. Wang, *ACS Appl. Mater. Interfaces*, 2013, **5**, 8217–8224.
200 M.-H. Yeh, L.-Y. Lin, C.-L. Sun, Y.-A. Leu, J.-T. Tsai, C.-Y. Yeh, R. Vittal and K.-C. Ho, *J. Phys. Chem. C*, 2014, **118**, 16626–16634.
201 Z. Xiang, X. Zhou, G. Wan, G. Zhang and D. Cao, *ACS Sustainable Chem. Eng.*, 2014, **2**, 1234–1240.
202 H.-W. Liu, S.-P. Liang, T.-J. Wu, H. Chang, P.-K. Kao, C.-C. Hsu, J.-Z. Chen, P.-T. Chou and I. C. Cheng, *ACS Appl. Mater. Interfaces*, 2014, **6**, 15105–15112.
203 B. Yang, X. Zuo, P. Chen, L. Zhou, X. Yang, H. Zhang, G. Li, M. Wu, Y. Ma, S. Jin and X. Chen, *ACS Appl. Mater. Interfaces*, 2015, **7**, 137–143.
204 B. Chen, J. Sha, W. Li, F. He, E. Liu, C. Shi, C. He, J. Li and N. Zhao, *ACS Appl. Mater. Interfaces*, 2016, **8**, 2495–2504.
205 G. S. Han, Y. H. Song, Y. U. Jin, J.-W. Lee, N.-G. Park, B. K. Kang, J.-K. Lee, I. S. Cho, D. H. Yoon and H. S. Jung, *ACS Appl. Mater. Interfaces*, 2015, **7**, 23521–23526.
206 N. A. Kumar, H.-J. Choi, Y. R. Shin, D. W. Chang, L. Dai and J.-B. Baek, *ACS Nano*, 2012, **6**, 1715–1723.
207 G. Xu, N. Wang, J. Wei, L. Lv, J. Zhang, Z. Chen and Q. Xu, *Ind. Eng. Chem. Res.*, 2012, **51**, 14390–14398.
208 D. Xu, Q. Xu, K. Wang, J. Chen and Z. Chen, *ACS Appl. Mater. Interfaces*, 2014, **6**, 200–209.
209 L. L. Zhang, X. Zhao, M. D. Stoller, Y. Zhu, H. Ji, S. Murali, Y. Wu, S. Perales, B. Clevenger and R. S. Ruoff, *Nano Lett.*, 2012, **12**, 1806–1812.
210 W. Li, Y. Bu, H. Jin, J. Wang, W. Zhang, S. Wang and J. Wang, *Energy Fuels*, 2013, **27**, 6304–6310.
211 C.-T. Hsieh, W.-Y. Lee, C.-E. Lee and H. Teng, *J. Phys. Chem. C*, 2014, **118**, 15146–15153.
212 L.-B. Xing, S.-F. Hou, J. Zhou, S. Li, T. Zhu, Z. Li, W. Si and S. Zhuo, *J. Phys. Chem. C*, 2014, **118**, 25924–25930.
213 V. Sahu, S. Shekhar, R. K. Sharma and G. Singh, *ACS Appl. Mater. Interfaces*, 2015, **7**, 3110–3116.
214 S. Cho, J. S. Lee and J. Jang, *ACS Appl. Mater. Interfaces*, 2015, **7**, 9668–9681.
215 R. Kumar, R. K. Singh, P. K. Dubey, D. P. Singh and R. M. Yadav, *ACS Appl. Mater. Interfaces*, 2015, **7**, 15042–15051.
216 K. Jo, M. Gu and B.-S. Kim, *Chem. Mater.*, 2015, **27**, 7982–7989.
217 J. Yang, E. Zhang, X. Li, Y. Yu, J. Qu and Z.-Z. Yu, *ACS Appl. Mater. Interfaces*, 2016, **8**, 2297–2305.
218 M. Wu, R. Kempaiah, P.-J. J. Huang, V. Maheshwari and J. Liu, *Langmuir*, 2011, **27**, 2731–2738.
219 J. S. Park, N.-I. Goo and D.-E. Kim, *Langmuir*, 2014, **30**, 12587–12595.
220 H. Zhang, C. Peng, J. Yang, M. Lv, R. Liu, D. He, C. Fan and Q. Huang, *ACS Appl. Mater. Interfaces*, 2013, **5**, 1761–1767.
221 G. Liu, H. Shen, J. Mao, L. Zhang, Z. Jiang, T. Sun, Q. Lan and Z. Zhang, *ACS Appl. Mater. Interfaces*, 2013, **5**, 6909–6914.
222 M. Zhang, Y. Cao, Y. Chong, Y. Ma, H. Zhang, Z. Deng, C. Hu and Z. Zhang, *ACS Appl. Mater. Interfaces*, 2013, **5**, 13325–13332.
223 C. L. Weaver, J. M. LaRosa, X. Luo and X. T. Cui, *ACS Nano*, 2014, **8**, 1834–1843.
224 K. Li, L. Feng, J. Shen, Q. Zhang, Z. Liu, S.-T. Lee and J. Liu, *ACS Appl. Mater. Interfaces*, 2014, **6**, 5900–5907.
225 A. Paul, A. Hasan, H. A. Kindi, A. K. Gaharwar, V. T. S. Rao, M. Nikkhah, S. R. Shin, D. Krafft, M. R. Dokmeci, D. Shum-Tim and A. Khademhosseini, *ACS Nano*, 2014, **8**, 8050–8062.
226 E. Song, W. Han, C. Li, D. Cheng, L. Li, L. Liu, G. Zhu, Y. Song and W. Tan, *ACS Appl. Mater. Interfaces*, 2014, **6**, 11882–11890.
227 X. Zhao, L. Yang, X. Li, X. Jia, L. Liu, J. Zeng, J. Guo and P. Liu, *Bioconjugate Chem.*, 2015, **26**, 128–136.

228 H. Kim, R. Namgung, K. Singha, I.-K. Oh and W. J. Kim, *Bioconjugate Chem.*, 2011, **22**, 2558–2567.
229 C. Xu, D. Yang, L. Mei, B. Lu, L. Chen, Q. Li, H. Zhu and T. Wang, *ACS Appl. Mater. Interfaces*, 2013, **5**, 2715–2724.
230 L.-N. Zhang, H.-H. Deng, F.-L. Lin, X.-W. Xu, S.-H. Weng, A.-L. Liu, X.-H. Lin, X.-H. Xia and W. Chen, *Anal. Chem.*, 2014, **86**, 2711–2718.
231 X.-P. He, Q. Deng, L. Cai, C.-Z. Wang, Y. Zang, J. Li, G.-R. Chen and H. Tian, *ACS Appl. Mater. Interfaces*, 2014, **6**, 5379–5382.
232 R.-C. Huang, W.-J. Chiu, Y.-J. Li and C.-C. Huang, *ACS Appl. Mater. Interfaces*, 2014, **6**, 21780–21787.
233 D. He, X. He, K. Wang, Z. Zou, X. Yang and X. Li, *Langmuir*, 2014, **30**, 7182–7189.
234 S. Z. Nergiz, N. Gandra, S. Tadepalli and S. Singamaneni, *ACS Appl. Mater. Interfaces*, 2014, **6**, 16395–16402.
235 L. Yang, Y.-T. Tseng, G. Suo, L. Chen, J. Yu, W.-J. Chiu, C.-C. Huang and C.-H. Lin, *ACS Appl. Mater. Interfaces*, 2015, **7**, 5097–5106.
236 T. Demeritte, B. P. Viraka Nellore, R. Kanchanapally, S. S. Sinha, A. Pramanik, S. R. Chavva and P. C. Ray, *ACS Appl. Mater. Interfaces*, 2015, **7**, 13693–13700.
237 N. Mauro, C. Scialabba, G. Cavallaro, M. Licciardi and G. Giammona, *Biomacromolecules*, 2015, **16**, 2766–2775.
238 J. Song, X. Yang, O. Jacobson, L. Lin, P. Huang, G. Niu, Q. Ma and X. Chen, *ACS Nano*, 2015, **9**, 9199–9209.
239 V. V. Singh, A. Martin, K. Kaufmann, S. D. S. de Oliveira and J. Wang, *Chem. Mater.*, 2015, **27**, 8162–8169.
240 Kenry, P. K. Chaudhuri, K. P. Loh and C. T. Lim, *ACS Nano*, 2016, **10**, 3424–3434.
241 J. Tang, Q. Chen, L. Xu, S. Zhang, L. Feng, L. Cheng, H. Xu, Z. Liu and R. Peng, *ACS Appl. Mater. Interfaces*, 2013, **5**, 3867–3874.
242 I. Ocsoy, M. L. Paret, M. A. Ocsoy, S. Kunwar, T. Chen, M. You and W. Tan, *ACS Nano*, 2013, **7**, 8972–8980.
243 D. Lin, T. Qin, Y. Wang, X. Sun and L. Chen, *ACS Appl. Mater. Interfaces*, 2014, **6**, 1320–1329.
244 Y.-W. Wang, A. Cao, Y. Jiang, X. Zhang, J.-H. Liu, Y. Liu and H. Wang, *ACS Appl. Mater. Interfaces*, 2014, **6**, 2791–2798.
245 J. He, X. Zhu, Z. Qi, C. Wang, X. Mao, C. Zhu, Z. He, M. Li and Z. Tang, *ACS Appl. Mater. Interfaces*, 2015, **7**, 5605–5611.
246 S. Prezioso, F. Perrozzi, L. Giancaterini, C. Cantalini, E. Treossi, V. Palermo, M. Nardone, S. Santucci and L. Ottaviano, *J. Phys. Chem. C*, 2013, **117**, 10683–10690.
247 Y. Liu, D. Yu, C. Zeng, Z. Miao and L. Dai, *Langmuir*, 2010, **26**, 6158–6160.
248 X. Liu, R. Aizen, R. Freeman, O. Yehezkeli and I. Willner, *ACS Nano*, 2012, **6**, 3553–3563.
249 R. Cheng, Y. Liu, S. Ou, Y. Pan, S. Zhang, H. Chen, L. Dai and J. Qu, *Anal. Chem.*, 2012, **84**, 5641–5644.
250 Y. Tu, W. Li, P. Wu, H. Zhang and C. Cai, *Anal. Chem.*, 2013, **85**, 2536–2542.
251 Y. Wang, Z. Li, T. J. Weber, D. Hu, C.-T. Lin, J. Li and Y. Lin, *Anal. Chem.*, 2013, **85**, 6775–6782.
252 S.-R. Ryoo, J. Lee, J. Yeo, H.-K. Na, Y.-K. Kim, H. Jang, J. H. Lee, S. W. Han, Y. Lee, V. N. Kim and D.-H. Min, *ACS Nano*, 2013, **7**, 5882–5891.
253 X. Liu, F. Wang, R. Aizen, O. Yehezkeli and I. Willner, *J. Am. Chem. Soc.*, 2013, **135**, 11832–11839.
254 J. Huang, Z. Wang, J.-K. Kim, X. Su and Z. Li, *Anal. Chem.*, 2015, **87**, 12254–12261.
255 Q. Zhao, Y. Zhou, Y. Li, W. Gu, Q. Zhang and J. Liu, *Anal. Chem.*, 2016, **88**, 1892–1899.
256 J. Song, L. Xu, C. Zhou, R. Xing, Q. Dai, D. Liu and H. Song, *ACS Appl. Mater. Interfaces*, 2013, **5**, 12928–12934.
257 G.-L. Wang, X. Xu, X. Wu, G. Cao, Y. Dong and Z. Li, *J. Phys. Chem. C*, 2014, **118**, 28109–28117.
258 W. Ren, Y. Fang and E. Wang, *ACS Nano*, 2011, **5**, 6425–6433.
259 S. Borini, R. White, D. Wei, M. Astley, S. Haque, E. Spigone, N. Harris, J. Kivioja and T. Ryhänen, *ACS Nano*, 2013, **7**, 11166–11173.
260 S.-H. Hwang, D. Kang, R. S. Ruoff, H. S. Shin and Y.-B. Park, *ACS Nano*, 2014, **8**, 6739–6747.
261 H.-W. Yu, H. K. Kim, T. Kim, K. M. Bae, S. M. Seo, J.-M. Kim, T. J. Kang and Y. H. Kim, *ACS Appl. Mater. Interfaces*, 2014, **6**, 8320–8326.
262 K. Paek, H. Yang, J. Lee, J. Park and B. J. Kim, *ACS Nano*, 2014, **8**, 2848–2856.
263 J. Wang, S. Rathi, B. Singh, I. Lee, H.-I. Joh and G.-H. Kim, *ACS Appl. Mater. Interfaces*, 2015, **7**, 13768–13775.